4

STOCHASTIC MODELS OF FRACTURE SYSTEMS AND THEIR USE IN FLOW AND TRANSPORT MODELING

Jean-Paul Chilès
Bureau de Recherches Géologiques et Minières
Orléans, France

Ghislain de Marsily
Université Pierre et Marie Curie
Paris, France

Fluid flow studies of fractured rocks require three-dimensional modeling of the fracture system. The complexity of reality does not allow a complete description of the actual field. It is therefore necessary to use stochastic models. The first task is the statistical study of the fracture population: identification of sets and distribution of orientation, size, and aperture. The second one is the choice of a network model: random planes, random discs, or models derived by mixing, clustering and regionalization of parameters. The third step is the study of the geometry of the single fracture: the shape of the fracture walls and of the channels. The fourth step is the derivation of the equations for fluid flow and solute transport in the network model. These various aspects are reviewed, including the conditioning of 3D simulations to the data. Emphasis is laid on the determination of the parameters by means of morphological, statistical, geostatistical and fractal tools that can be used with 1D information (boreholes) or 2D data (outcrops and drift walls); the use of hydraulic testing in boreholes and of tracer tests for determining flow and transport parameters is also presented. The link between geometry, connectivity, percolation theory, and flow is examined. Stationarity and ergodicity assumptions used for modeling stochastic fracture systems are discussed.

4.1 INTRODUCTION

The rock mechanics, flow and transport properties of hard rocks depend mainly on the characteristics of the fracture field, which ought to be considered separately from the matrix. Applications are increasingly complex, and some involve a complete description of the fracture

field (e.g., Long, 1986). As fractures are not directly accessible in their entirety, but only at their intersections with boreholes, outcrops or drifts, one of the first steps in the study of a given site is modeling and simulation of the fracture field.

This modeling can be done at various scales, e.g., large faults, fractures, and microfissures. This chapter deals with the scale ranging from tens of centimeters to tens of meters. Large faults (up to a kilometer) are not found very often and are assumed to have been identified by means of a deterministic approach. In contrast, microfissures (millimetric or centimetric in scale) are considered as a property of the matrix, and their influence on flow is summarized through an equivalent continuous medium. Thus, our aim is modeling at the metric scale. Of course, the method is general and can easily be transposed to another scale (e.g., at the microfissure scale) in order to define an equivalent continuous medium.

Whatever the scale, two distinct features can be studied:

i) the fracture network: each element is considered as relatively simple (e.g., a planar fracture) and stress is laid on the imbrication of the various elements;

ii) the single fracture: generally, an open fracture is not a pair of parallel plates: there are voids and contact areas that depend on stress, and this has an enormous influence on conductivity (Feuga, 1986).

The main part of this chapter (sections 4.2 to 4.10) is focused on the fracture network. A 3D domain, even limited, can correspond to several thousand or over a million fractures. Few of these fractures intersect the boreholes, outcrops, or drift walls where the network is observed, which is the reason why deterministic modeling is not possible; hence stochastic modeling will be considered. The mathematical morphology approach is the reference, but simpler methods are usually used. Statistical tools describe the fracture population. Geostatistical tools and fractal methods are used to study the regionalized behavior of the network. The combination of these approaches leads to a realistic modeling and simulation of the 3D network. All these aspects of modeling are presented, with a final section devoted to the conditioning of a 3D simulation by observed 1D or 2D fracture intersections.

Section 4.11 is devoted to the single fracture. The approach can be global (definition of an average permeability) or local (2D modeling of both surfaces and void, using geostatistical or fractal methods). Both are presented. Section 4.12 briefly examines the link between fracture field, connectivity, and flow. The relationship between percolation theory and connectivity is introduced in section 4.13.

Section 4.14 describes how a discrete fracture flow model is built, calibrated, and used, and section 4.15 addresses the same issues for a transport model. Finally section 4.16 describes another stochastic fracture model based on the representation of a continuous equivalent medium.

In the study of the fracture network, fractures are considered as planar. This is, of course, a simplification, but one that does not usually modify the conclusions on connectivity or stability. According to the scale, they will be considered as either infinite or convex, so that fracture traces are either straight lines or segments.

4.2 MATHEMATICAL MORPHOLOGY APPROACH

Mathematical morphology (Matheron, 1975; Serra, 1982) provides a means of fully characterizing a fracture network. As we are considering stochastic models, let us denote by A the (random) set of all the fractures (fracture walls and void spaces). If we neglect the aperture of the fractures, this set will be fully determined by the knowledge of the functional moment $Q(B)$ for any (nonrandom) set B, where $Q(B)$ is defined by:

$$Q(B) = \text{Prob}\{B \cap A = \varnothing\} = \text{Prob}\ \{B \text{ does not intersect any fracture}\} \qquad (4.2.1)$$

This characterization is the exact equivalence of the spatial law for random functions. The random set A is usually assumed to be stationary. $Q(B)$ is then unchanged by translation of B and can be estimated from the sole realization of the fracture network.

In practice it is not possible to consider any set B. Conrad and Jacquin (1973) used this approach to study a 2D network, with B being a segment, a disc, or a crown. The moments $Q(B)$ were measured with a texture analyzer. This is a very powerful method, which deserves to be rediscovered. Its implementation for 3D studies is not obvious and hence, other tools, less powerful but simpler, are usually used. Before presenting them, it is necessary to explain how data are collected.

4.3 TYPES OF SURVEY

There are three main types of survey:

4.3.1 Borehole Surveys

The measurements are usually made on oriented cores or deduced from resistivity logs. For each intersected fracture, one notes its location, orientation, existence of possible fill (nature, thickness), aperture, surface geometry, etc. Borehole measurements give information about the distribution of fracture orientation, the fracture density and its regionalization, the presence of fracture clusters. But only 2D surveys allow the evaluation of the fracture size, which is a major parameter in the study of the mechanical and hydraulic properties of the rock.

4.3.2 Scanline Surveys

This is an extension of the preceding technique to a 2D area. As for boreholes, only the fractures intersecting a line (usually a horizontal one), painted on an outcrop or on a batter, are collected. But each fracture is now represented by its trace, which can be measured (Fig. 4.3.1.a). This method is commonly used for pit batters and high bench walls that make it possible to observe long traces. The scanline is established about one meter above the bench level and, due to the presence of debris on the bench area, only the portion of trace occurring above the scanline is visible and measured (half-trace line sampling). If the batter is clean, it is of course better to also measure the length of the fracture below the line (full-trace sampling). In comparison with a borehole survey, two additional observations are required for each trace intersecting the line:

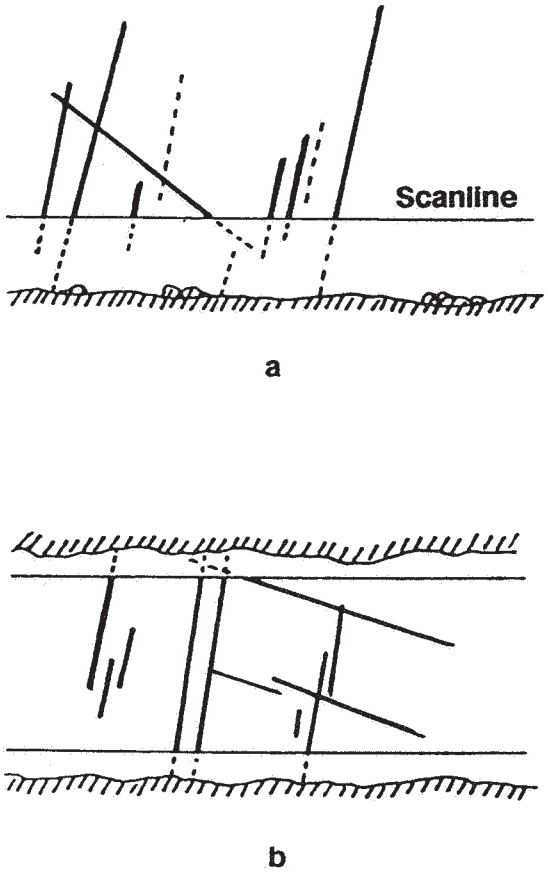

Figure 4.3.1. 2D survey of fracture traces: a) scanline survey; b) areal survey.

i) the coordinates (on the wall) of the apparent termination above the line (the half trace length will be deduced from this measurement and from the location of the intersection with the line); and

ii) whether or not the trace extends beyond the top of the batter.

Additional qualitative observations are noted, such as the termination type (in rock, or at the contact with another fracture) or the fracture relays. Vertical lines are also surveyed in order to collect data concerning subhorizontal fractures.

4.3.3 Areal Surveys

All traces intersecting a rectangle are collected (Fig. 4.3.1.b). The traces are censored to the rectangle, which means that if they extend beyond the rectangle, only their inner portion is considered. This method is recommended for drift or tunnel walls, but can be used for outcrops. As the height of the rectangle is limited to the wall height (commonly around two meters), the available information is reduced, and this type of survey makes it possible to retain all the available information. The same parameters are sampled as for a scanline survey, but the fracture is now represented by its full—possibly censored—trace; its location is characterized by the

coordinates of it two endpoints within the surveyed surface. The visible length of the trace can be deduced from these data. For each endpoint it must also be noted if it is really a termination of the fracture trace, or if the trace extends beyond the surveyed surface. The rectangle must be carefully delimited, for it is tempting not to collect traces that are at the foot or at the top of the drift.

4.4 STATISTICAL STUDY OF THE FRACTURES

4.4.1 Fracture Sets

The orientation of fractures, though not regular, is not purely random. Usually, many of the fractures observed in a single outcrop are approximately parallel to one or several planes. These fractures, which have approximately the same orientation, constitute a fracture set. The existence of sets is due to the fact that the orientation of fractures is related to tectonic history. The first tectonic event has created two or more conjugate sets of fractures, whereas the last events have usually reactivated previous fractures. It is best to study the various sets separately, as individual sets are expected to be more homogeneous than combined sets (e.g., the size or the aperture can differ from one set to another). A first task is to identify the various sets. This may not be easy, in particular because of the geometric bias associated with the data. This problem is first introduced below together with the definition and calculation of the fracture density, and will be developed later.

4.4.2 Fracture Density

The 3D fracture density d_3 (of all the fractures or of a given set) is the average fractured surface per unit rock volume. Similarly, the 2D fracture density d_2 on a planar surface is the average fractured length (of traces) per unit surface area; the 1D fracture density d_1 along a straight line is the average number of fracture intersections per unit length. Both d_1 and d_2 depend on the orientation of the line or plane considered, except in the case of isotropy of the fracture network. Therefore, the most interesting parameter is d_3. It can be obtained from a survey with boreholes or scanlines, with the help of a weighting of the observed fractures. In order to determine the correct weights, it is sufficient to consider the surveyed straight line of length L as a cylinder with a small section s (as is the case for a borehole). If n fractures intersect the line, and if the i^{th} fracture intersects it with an acute angle θ_i, then the fracture surface within the cylinder is $s/\sin\theta_i$. Hence we get:

$$d_3 = \frac{1}{Ls}\sum_{i=1}^{n}\frac{s}{\sin\theta_i} = \frac{1}{L}\sum_{i=1}^{n}\frac{1}{\sin\theta_i}$$

Similarly, for an areal survey, the plane can be considered as a very thin layer with thickness e. The surface, within the layer, of a fracture of trace length l_i within the surveyed rectangle, and acute angle θ_i with the plane, is $el_i/\sin\theta_i$. Hence, denoting the surveyed area as S, and the number of fractures intersecting the surveyed rectangle as n we get:

$$d_3 = \frac{1}{S} \sum_{i=1}^{n} \frac{l_i}{\sin \theta_i} = \frac{1}{S} \sum_{i=1}^{n} \frac{l_i}{\sin \theta_i}$$

(N.B.: Many authors also use the $1/\sin\theta_i$ weighting for an areal survey; this is only acceptable when one considers a set of infinite parallel fractures, for which l_i is constant, except at the edges.)

If all the fractures are parallel, the angle θ_i is constant and can be denoted as θ. The link between 1D and 3D fracture densities is then $d_1 = d_3 \sin\theta$. A similar relationship between 2D and 3D fracture densities exists. In all cases, the apparent density d_1 or d_2 is smaller than the true density d_3. The only exception is the case where the borehole, outcrop or wall is orthogonal to the fracture set.

In the case where the fracture orientations are purely random, the mean value of $\sin\theta$ between a fracture plane and a survey line is 1/2. It is $\pi/4$ between a fracture plane and a survey plane. The 1D, 2D, and 3D fracture densities are then linked by the relations:

$$d_1 = \frac{1}{2} d_3 \qquad d_2 = \frac{\pi}{4} d_3$$

4.4.3 Definition of the Orientation

a) Strike and Dip

The orientation of a fracture is usually expressed by its strike and dip. The strike is the trace of the intersection of the fracture with a horizontal plane; its direction can be specified by its azimuth, counted in degrees clockwise from the north. For example, the azimuth 300° corresponds to the direction N60W. The dip (or inclination, or plunge) is the magnitude of the angle between the fracture and a horizontal plane expressed in degrees.

If the strike is oriented so that the dip plunges on the right-hand side, the strike azimuth (a unique value between 0 and 360°) and the dip angle (between 0 and 90°) define the fracture orientation. If the strike is not oriented, and hence is defined up to 180°, it is necessary to also specify the approximate orientation of the dip (N, S, E, W). In the following, the strike is considered as oriented. There are also other systems: some authors use the dip direction instead of the strike (dip direction = strike direction + 90°), others express the angles in grades instead of degrees.

For calculations, it is more convenient to characterize the orientation by a unit vector orthogonal to the fracture plane (the fracture is translated so as to pass through the origin 0). This unit vector is defined either in polar coordinates or by its direction cosines.

b) Polar Coordinates

The polar coordinates of a unit vector OP are usually defined by the angle θ between the z axis and vector OP (colatitude), and by the angle ϕ between the x axis and the projection of OP on the xOy plane (longitude), counted anticlockwise (Fig. 4.4.1). For the unit vector orthogonal to a fracture plane and oriented upwards, the link between strike and dip and the polar coordinates, is the following:

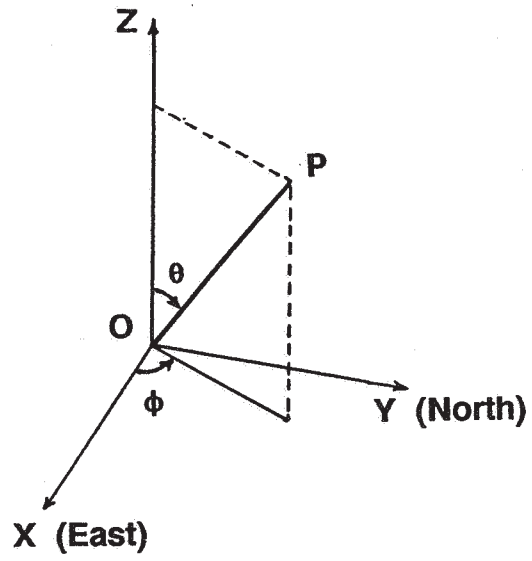

Figure 4.4.1. Definition of the polar coordinates of a unit vector orthogonal to the fracture plane.

θ = dip angle $\phi = 2\pi$ - strike azimuth

c) Direction Cosines

The direction cosines (u, v, w) of vector OP are the components of the vector. These components are equal to the cosines of the angles a, b, c, which the vector OP makes with the positive directions of the coordinate axes. The relationship between polar coordinates and direction cosines is the following:

$$u = \sin\theta\cos\phi \qquad v = \sin\theta\sin\phi \qquad w = \cos\theta \tag{4.4.1}$$

4.4.4 Projections and Polar Diagrams

Techniques to represent fracture orientations are well known. A comprehensive presentation can be found in Terzaghi (1965) with references to other authors. The main elements are presented in the following.

a) Poles and Axial Points

In order to visualize and to define the various fracture sets observed in an area, fracture orientations may be represented by points on the projection of a reference sphere with unit radius and center at the origin. One does not represent the actual fracture, but the direction of the normal to the fracture plane. More precisely, the reference sphere diameter that is orthogonal to the fracture plane intersects the reference sphere at two points, one in the lower hemisphere, the other in the upper hemisphere. These points are called the poles of the fracture (Fig. 4.4.2). Obviously,

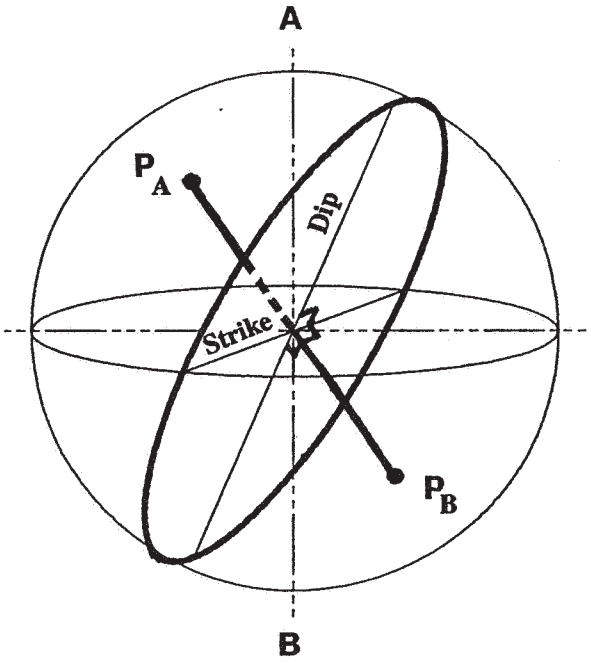

Figure 4.4.2. Upper pole P_A and lower pole P_B of a fracture on the reference sphere.

it is enough to retain only one of them. For the purpose of visualization, we will use the pole of the lower hemisphere, although the other one is sometimes used; the other pole will occasionally be used in subsequent sections.

Linear elements, such as the axis of a drill hole or a drift, may be represented by one of the points at which an identically oriented diameter of the sphere would meet the surface of the sphere. Such a point is called the axial point of the linear element to which it refers. It coincides with the pole of the fractures that are orthogonal to the linear elements.

The poles and axial points located on the surface of the reference sphere may be projected onto a plane by one or several methods. Those most commonly used are the Lambert equal-area and the stereographic projections.

b) Equal-Area Projection and Schmidt Diagram

The Lambert equal-area, or simply equal-area, projection is illustrated by Fig. 4.4.3.a. The projection plane is the plane tangent to the lower point B of the vertical diameter of the reference sphere. The vector joining B to the fracture lower pole P is rotated in its vertical plane in such a way as to become a vector BP' in the projection plane. In the 2D polar coordinates of the projection plane centered on B, the coordinates of P' are:

$$\text{polar distance: } \rho = 2\sin(\theta'/2) \quad \text{polar angle: } \psi = \varepsilon'$$

$$\text{with } \theta' = \pi - \theta \quad \phi' = \phi \pm \pi$$

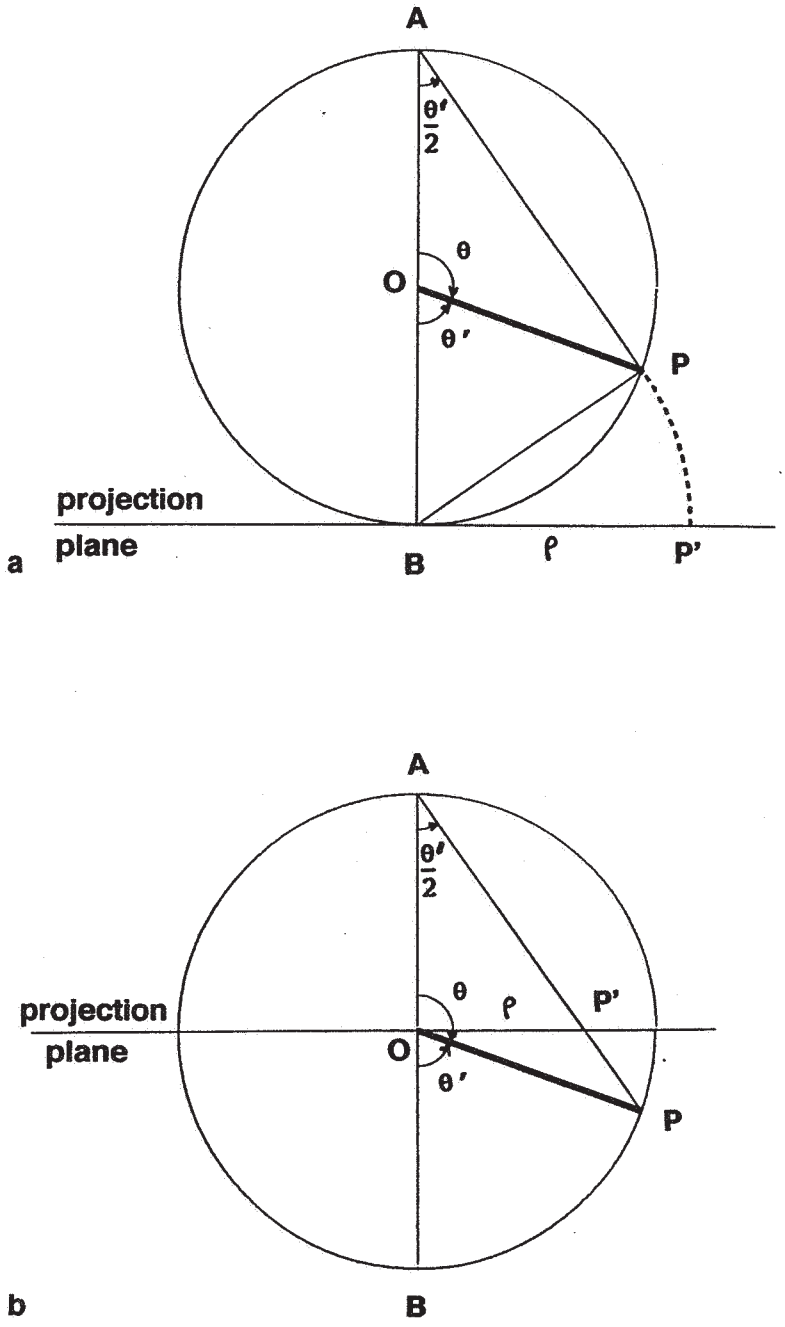

Figure 4.4.3. Pole projections: a) equal-area projection (in the vertical plane of the pole); b) stereographic projection (in the vertical plane of the pole).

In this projection, two equal areas in the projection represent two equal areas in the reference hemisphere. This feature is advantageous in the statistical study of the fracture density. A counterpart of this projection lies in the distortion, which is greatest at the circumference of the projection circle. Plotting the fracture poles according to this projection is called a Schmidt diagram. Poles near the center of the diagram correspond to subhorizontal fractures, and those near the circumference correspond to subvertical fractures. For a lower-hemisphere projection, the left-hand poles represent eastward dipping fractures, whereas right-hand poles represent

westward dipping fractures (in case of an upper-hemisphere projection, the diagram would be transformed according to a symmetry around the center of the projection circle, and hence, the opposite applies).

c) Stereographic Projection and Wulff Diagram

The equal-angle stereographic, or simply stereographic projection, is illustrated in Fig. 4.4.3.b. The projection plane is now the horizontal xOy plane to which the center O of the sphere belongs. The projection P' of the fracture pole P is the intersection of the line joining the upper point A of the vertical diameter to the fracture pole P with the xOy plane. In the 2D polar coordinates of plane xOy, the coordinates of P' are:

$$\text{polar distance: } \rho = tg(\theta'/2) \qquad \text{polar angle: } \psi = \phi'$$

An advantage of the stereographic projection is that it presents no distortion; a small circular area drawn anywhere on the reference sphere is represented by a very nearly circular area in the stereographic projection. However, an area of a given size on the reference sphere is represented in the stereographic projection by an area the size of which increases conspicuously with the distance from the center of the projection circle. Plotting the poles according to a stereographic projection produces a Wulff diagram. Its interpretation is similar to that of a Schmidt diagram. In our domain, the Schmidt diagram is usually preferred, as its equal-area property is very convenient for the statistical study of the fracture density and the delineation of fracture sets.

d) Contoured Polar Diagrams

In general, the results of a fracture survey are most conveniently represented by a contoured polar diagram, as illustrated in Fig. 4.4.4.a. A unit circle (small compared to the reference sphere) is moved systematically from position to position, across the reference sphere. In each position, the number of poles inside the unit circle is counted. This number, or its ratio to the total number of fractures, is recorded on the diagram at the projection of the center of the unit circle. From this new data set, the fracture density is interpolated and plotted. Diggle and Fisher (1985) present variants of this method with numerous references and a program.

e) Geometric Bias

When such a diagram is interpreted, it is necessary to account for the geometric bias resulting from the orientation of the surveyed boreholes or outcrops. Fractures that are normal to the surveyed line or surface occur more often than oblique fractures. This bias can be reduced by collecting data from boreholes, outcrops, or drifts with various orientations. On the contrary, if the orientation diagram corresponds to a single borehole or outcrop, it may be sufficient to represent the axial pole of the surveyed line or the pole of the outcrop and to read the diagram accordingly. In other cases, it is advisable to weight the data. The bias has the same origin as in the study of the 3D fracture density, and hence the weights are the same ($1/\sin\theta_i$ for a borehole or scanline survey, $1_i/\sin\theta_i$ for an areal survey). Figure 4.4.4 presents an example of the difference between a weighted and a nonweighted diagram, used by Courrioux and Jacquot (1984).

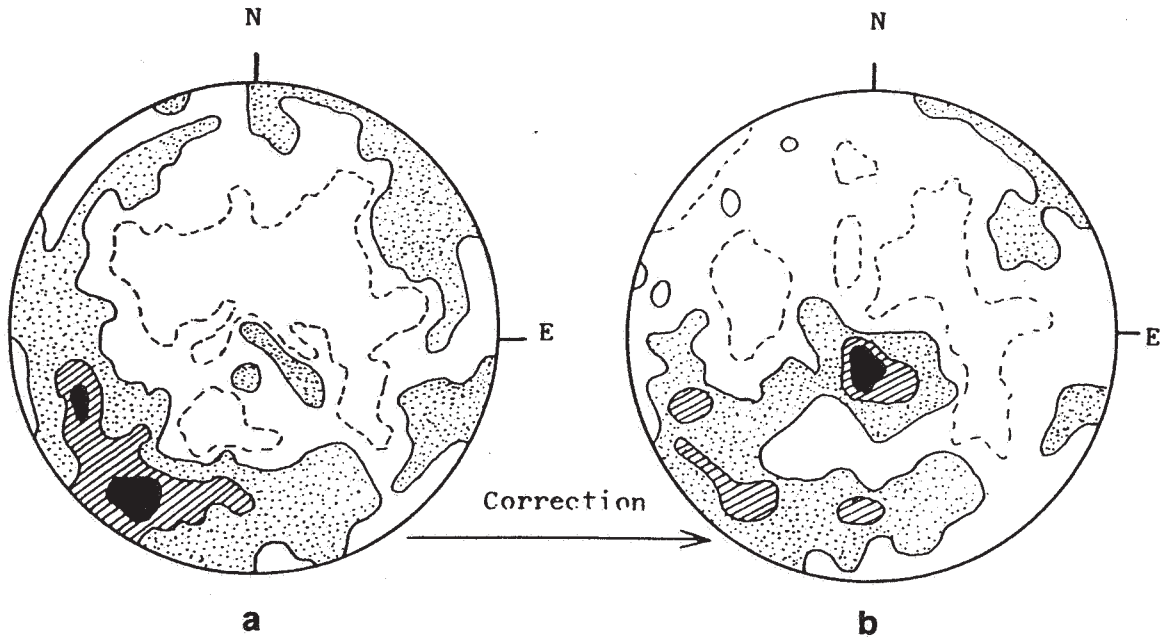

Figure 4.4.4. Contoured polar diagram: a) non-weighted; b) weighted. After Courrioux and Jacquot (1984).

This weighting is valid only under ideal conditions, with a strictly planar outcrop or drift wall, strictly planar fractures, and perfect angle measurements. As these conditions never occur, the corrective factor (inversely proportional to $\sin\theta_i$) has its own uncertainty, which is small if θ_i lies around 90°, but becomes infinite if θ_i equals 0°: as the surface of drift is not strictly planar, it is possible to observe fractures that have the same orientation as the mean drift wall orientation, even if this is impossible in theory. Thus, most authors recommend not using any fracture with θ_i less than 20 or 30 degrees. Otherwise the corrective factor must take account of the actual measurement conditions:

i) the non-planarity of outcrops and fractures can be accounted for in a similar way as the cut effect in petrographic diagrams (Courrioux and Jacquot, 1984). For example, the convex envelope of a fracture trace can be considered as an ellipse with a small eccentricity e (ratio small axis/great axis); in this case, $(\sin^2\theta_i + e^2 \cos^2\theta_i)^{1/2}$ replaces $\sin\theta_i$ in the expression of the corrective factor;

ii) the uncertainty concerning θ_i can be accounted for by randomization according to the measurement precision (see Yow, 1987).

Note that these remarks also apply to the estimation of the 3D density.

4.4.5 Identification of Fracture Sets

The Schmidt or Wulff diagram shows the existence of different sets. Several cluster-analysis methods have been developed to automatically define the various sets (e.g., Bailey, 1975; Schaeben, 1984). However, these methods do not take into account the geometric bias nor the

measurement errors, and it is therefore sufficient to define the various sets from a visual inspection of the diagram. Moreover, structural geologists can usually relate fractures to tectonic history, which further helps in the definition of sets.

4.4.6 Modeling of the Orientation Distribution

The statistical modeling of directional data has been studied for a long time. See for example Mardia (1972) and his references to previous authors. The elements necessary for our studies are presented later. The most commonly used models for spherical orientations concerning a fracture set are the truncated Fisher, the Bingham, and the uniform distributions. The expression of these distributions is simpler when the coordinate system, linked with the reference sphere, is changed in such a way that the "new" north pole coincides with the mean direction of the given fracture set.

Change of Reference System

Denote (θ_0,ϕ_0) as the mean orientation in the reference system (Ox,Oy,Oz) with spherical coordinates (θ,ϕ). The change from this system to a reference system (Ox', Oy', Oz') with spherical coordinates (θ',ϕ'), such that the mean orientation coincides with the new north pole axis $\theta' = 0$, can be obtained by a single rotation, of angle θ_0, which leads Oz to Oz'. In this case (θ',ϕ') is defined from (θ,ϕ) by:

$$\begin{aligned} \sin\theta'\cos\phi' &= \cos\theta_0 \quad \cos(\phi-\phi_0)\sin\theta - \sin\theta_0\cos\theta \\ \sin\theta'\sin\phi' &= \quad\quad \sin(\phi-\phi_0)\sin\theta \\ \cos\theta' &= \sin\theta_0 \quad \cos(\phi-\phi_0)\sin\theta + \cos\theta_0\cos\theta \end{aligned}$$

The "new" great circle with longitude $\phi' = 0$ is the "old" great circle with longitude $\phi = \phi_0$.

For the reverse transformation, a rotation of angle $\theta'_0 = -\theta_0$ around the Oy' axis would lead the Oz' axis to the "old" north pole axis, and give θ, $\phi - \phi_0$. Hence (θ,ϕ) is defined from (θ',ϕ') by:

$$\begin{aligned} \sin\theta\cos(\phi-\phi_0) &= \cos\theta_0 \quad \cos\phi'\sin\theta' + \sin\theta_0\cos\theta' \\ \sin\theta\sin(\phi-\phi_0) &= \quad\quad \sin\phi'\sin\theta' \\ \cos\theta &= -\sin\theta_0 \quad \cos\phi'\sin\theta' + \cos\theta_0\cos\theta' \end{aligned}$$

Estimation of the Mean Direction

There are sophisticated methods for estimating the mean direction (θ_0,ϕ_0), e.g., Mancktelow (1981). Because of the uncertainties associated with the definition of the "direction" of a fracture and with the measurement itself, and due to the geometric bias (usually not taken into account in the sophisticated methods), it is sufficient to identify the mean direction with the direction of the weighted sum of all the unit vectors orthogonal to the fractures of the set (use relations 4.4.1 to compute the components of the unit vectors). In principle, each unit vector must be weighted according to the geometric bias corrective factor. In the study of undirected orientations, the

choice of the direction of each unit vector must be consistent: starting from an approximate value of (θ_0, ϕ_0), each (θ_i, ϕ_i) is chosen such that both associated unit vectors form an acute angle (if this is not the case, take $\pi-\theta_i$ and $\phi_i \pm \pi$).

Uniform Distribution

If the directions are uniformly distributed on the upper hemisphere, the probability density function (pdf) associated with a surface element ds is $ds/(2\pi)$. Expressed in spherical coordinates, as the surface associated with $d\theta$ and $d\phi$ is $ds = \sin\theta\, d\theta\, d\phi$, the bivariate pdf of the polar coordinates θ, ϕ referred to the reference sphere is:

$$f(\theta,\phi)=\frac{1}{2\pi}\sin\theta \qquad 0<\theta<\pi/2 \qquad 0<\phi<2\pi$$

θ and ϕ are independently distributed, ϕ is uniformly distributed on $[0,2\pi]$, and $\cos\theta$ uniformly distributed on [0,1].

Fisher Distribution

This is an isotropic nonuniform distribution. When referred to new axes Ox', Oy', Oz', such that Oz' is the pole of the mean direction, the bivariate pdf of the polar coordinates (θ', ϕ') referred to the reference sphere is:

$$f(\theta',\phi')=\frac{1}{2\pi}\frac{k\sin\theta'}{e^k-e^{-k}}\exp(k\cos\theta') \qquad 0<\theta'<\pi \qquad 0<\phi'<2\pi$$

k is a concentration parameter: for $k = 0$, the mass is uniformly distributed; for large k, the mass is concentrated on a small portion of the sphere around the pole of the mean direction.

In our case, undirected orientations are considered, and the Fisher distribution must be truncated to $\theta' = \pi/2$ (it is then known as the Arnold distribution). In this case, the multiplying factor $k/(e^k - e^{-k})$ must be replaced by $k/(e^k - 1)$. It can be truncated to a lower value θ'_0, with the corresponding multiplying factor $k/(\exp(k) - \exp(k\cos\theta'_0))$

From the expression of the pdf, it follows that θ' and ϕ' are independent random variables: ϕ has a uniform distribution on $[0,2\pi]$, and $T = 1 - \cos\theta'$ has a truncated exponential distribution $ke^{-kt}/(1 - e^{-kt_0})$, where $t_0 = 1 - \cos\theta'_0$ is the point of truncation (usually $\theta'_0 = \pi/2$, and hence $t_0 = 1$). As k is usually high, the exponential tail probability beyond the truncation point, e^{-kt_0}, is negligible, and the distribution of T can be regarded as exponential, with mean k. This provides an easy estimation of k, and enables the user to check whether the bivariate distribution of (θ,ϕ) can be considered as truncated Fisher (see Lewis and Fisher, 1982).

Bingham Distribution

Expressed in the polar coordinates (θ',ϕ'), it has the bivariate pdf:

$$f(\theta',\phi')=\frac{1}{2\pi}\frac{\sin\theta'}{M_k}\exp(k\cos^2\theta') \qquad 0<\theta'<\pi/2 \qquad 0<\phi'<2\pi$$

with

$$M_k = \int_0^1 e^{kt^2}\, dt$$

More general forms exist of the Bingham distribution, which can model anisotropic distributions (see Mardia, 1972).

Gaussian Distribution in a Projection Plane

It is also possible to project (θ',ϕ') in the plane tangent to the north pole (upper hemisphere projection) by using an equal-area projection, a stereographic projection or simply the intersection of the direction (θ',ϕ') with this tangent plane (projection from the sphere center). The projection has in this case the following 2D polar coordinates:

polar distance:	equal-area projection:	$\rho = 2\sin(\theta'/2)$
	stereographic projection:	$\rho = tg(\theta'/2)$
	projection from center:	$\rho = tg\theta'$
polar angle:		$\psi = \phi'$

and the Ox axis in the projection plane is the great circle with longitude $\phi' = 0$.

The advantage of the last projection lies in that the half-hemisphere is represented by the whole plane. So, as suggested by Grossman (1985), it is possible to model the orientation with a bivariate Gaussian distribution, which is easy, even in case of anisotropy.

4.4.7 Trace Length and Fracture Size

If fractures cannot be considered as infinite at the scale of the study, the distribution of their size largely determines the frequency of intersections and hence the mechanical and hydraulic behavior of the rock mass (existence of distinct blocks, flow, etc.). For a fixed 3D fracturation density, there is a better connectivity with a few large fractures than with many small ones. In practice, it is not possible to observe the exact size of a fracture. A 2D survey, however, provides the trace-length distribution, which is linked with the fracture-size distribution, but the experimental histogram of trace length is affected by several biases that have to be corrected.

Biases of the Experimental Trace-Length Distribution

As pointed out by several authors (see Baecher and Lanney, 1978), there are three main causes of bias:

i) **Censoring.** When one or both terminations of a trace are not observable, as is often the case on drift walls for subvertical fractures, the length recorded is a censored length, being shorter than the true length; hence, a reduction of the histogram dispersion.

ii) **Truncation.** Traces that are shorter than some cut-off length are not recorded, either because they are considered of secondary importance or because it is difficult to discriminate between natural fractures and fractures due to mining when they are small; hence, a truncation of the histogram.

iii) **Size.** First consider a horizontal scanline survey of fractures with the same orientation; if the level of the scanline is randomized, it clearly appears that the probability of intersecting a given trace is proportional to its length. In the calculation of the experimental histogram, each trace appears as weighted by its length: it is a histogram in measure and not in number (see e.g., Serra, 1982). In the case of an areal survey, the weighting is more complex, but the phenomenon remains.

Derivation of the True Trace-Length Distribution

These biases are well-known, and methods for deriving the true (in number) mean or the underlying distribution have been developed (Cruden, 1977; Baecher and Lanney, 1978; Pahl, 1981; Laslett, 1982, who presents most methods). Considering an areal survey, both Pahl and Laslett separate the traces into three classes according to the number of visible terminations (0, 1, or 2). Pahl proposes a distribution-free estimation method of the mean trace length, whereas Laslett presents a parametric method (maximum likelihood) for the estimation of the trace length distribution. Pahl's method can be easily extended to the estimation of the distribution (Massoud, 1987); here this last method is presented.

Consider a set of traces with the same apparent (2D) orientation (if the orientation varies, the result will simply have to be randomized), and consider the areal survey of a drift wall within a rectangle of length L and height H. More precisely, in order to avoid edge effects, the survey area is a parallelogram of height H, whose lateral sides are parallel to the considered traces (Fig. 4.4.5). Note:

θ	angle between the base-line and the traces
τ_2	density of trace centers within the rectangle plane
$F(l)$	cumulative distribution function (cdf) of trace length (in number)
$f(l)$	probability density function (pdf) associated with $F(l)$
N_0	number of traces with 0 visible termination (all with length $a = H/\sin\theta$)
$N_1(dl)$	histogram of censored length of traces with 1 visible termination
$N_2(dl)$	histogram of length of traces with 2 visible terminations

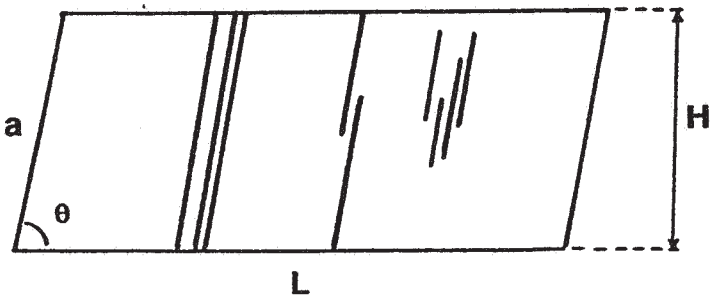

Figure 4.4.5. Derivation of the true trace-length distribution in the case of an areal survey; refer to text for explanations.

It is easily proved, using geometric probability arguments, that if measurements are made up to the limits of the parallelogram, these histograms have the following expectation:

$$\begin{aligned} E[N_0] &= \tau' \int_a^\infty [1-F(l')]\,dl' && (l=a) \\ E[N_1(dl)] &= 2\tau'[1-F(l)]\,dl && (l<a) \\ E[N_2(dl)] &= \tau'(a-l)\,f(l)\,dl && (l<a) \end{aligned} \tag{4.4.2}$$

where $\tau' = \tau_2 L \sin\theta$ and $a = H/\sin\theta$.

These results take account of the various types of bias. If τ_2 is known, the histograms of N_1 and N_2 lead to two different estimations of the trace-length distribution for $l < a$, and N_0 makes it possible to fit the behavior of the distribution for $l > a$. In practice, the density τ_2 of trace centers is not exactly known (the actual center of the censored traces can be located outside the surveyed rectangle), and one simultaneously determines density τ_2 and distribution $F(l)$ by trial and error, in such a way as to get a good fit of the three theoretical histograms on the three experimental ones.

In the case of a scanline survey, the method is the same, except that only N_0 and N_1 are available. If H is the height of the bench above the scanline, the mathematical expectation of the experimental histograms becomes:

$$\begin{aligned} E[N_0] &= \tau' \int_a^\infty [1-F(l')]\,dl' && (l=a) \\ E[N_1(dl)] &= \tau'[1-F(l)]\,dl && (l<a) \end{aligned} \tag{4.4.3}$$

As explained below, the method is distribution-independent, but, in practice, one tries several classical models such as the exponential and the lognormal distributions.

c) Derivation of the Fracture-Size Distribution

Knowledge of the trace-length distribution is not enough to determine the fracture-size distribution, unless assumptions are made regarding the shape of fractures. A particularly simple case is the one where fractures can be considered as discs. The 3D parameters (3D density of disc centers τ, pdf $h(D)$ of disc diameter) and the 2D parameters (2D density of trace centers τ_2, pdf $f(l)$ of trace length) are then linked by simple relations that were developed for fractures by Warburton (1980) and are standard results in the field of stereology (Stoyan et al., 1987, Ch. 11):

$$\begin{aligned} \tau_2 &= \bar{D}\,\tau \\ f(l) &= \frac{l}{\bar{D}} \int_l^\infty \frac{h(D)}{\sqrt{D^2 - l^2}}\,dD \end{aligned} \tag{4.4.4}$$

where D is the mean disc diameter

$$\bar{D} = \int_0^\infty D\,h(D)\,dD$$

The relation (4.4.4) between pdf's can be integrated to get the cdf $F(l)$, which is more useful:

$$F(l) = 1 - \frac{1}{\bar{D}} \int_{l}^{\infty} \sqrt{D^2 - l^2}\, h(D)\, dD \qquad (4.4.5)$$

The density of disc centers τ should not be confused with the 3D fracturation density d_3. They are linked by the relationship $d_3 = \tau S$, where S is the average disc surface, i.e.,

$$S = \pi / 4 \left(\bar{D}^2 + \sigma_D^2 \right)$$

where σ_D is the disc diameter standard deviation.

From relation (4.4.5), it is known that, even if the disc-diameter distribution is not lognormal, the trace-length distribution tends to look lognormal. The inversion of relation (4.4.5) to derive the cdf $H(D)$ from the cdf $F(l)$ is possible in theory, but unstable in practice; it is an ill-posed problem, as pointed out by O'Sullivan (1986) in a very similar case. Therefore in practice one simply tries to fit an exponential or lognormal distribution. This step can be regrouped with the previous step (derivation of the true trace length distribution): combining relations (4.4.2) or (4.4.3) and (4.4.5), one chooses a disc-diameter distribution (type, mean D, standard deviation σ_D if necessary) and a 3D density of disc centers τ, such that the theoretical histograms of N_0, N_1, and possibly N_2, fit the corresponding theoretical ones.

4.4.8 Aperture and Thickness

Aperture is an important parameter for flow calculations, but it is difficult to handle, for two main reasons:

i) aperture is not constant: there are voids and contact areas, and flow between two parallel plates separated by the mean aperture has nothing in common with the actual flow;

ii) because of stress release, the measured aperture has nothing in common with an in-situ aperture.

Thus, the study of the apparent aperture is unsatisfactory. Indirect methods are used, e.g., water injection tests (Snow, 1970; see also Ch. 9). In some cases, however, the fracture is filled with calcite or another material, and the aperture is replaced by a thickness, which is not affected by stress release and is commonly found to have a lognormal distribution.

4.4.9 Correlations between Parameters

All parameters can be correlated, but, as the fractures have been separated into several sets, the correlations are usually low. An important exception is the thickness, which is usually found to be strongly positively correlated with the fracture size (see Loiseau, 1987, who studied fractures in gneiss and found correlation coefficients around 0.90 between thickness and trace length).

4.5 BASIC NETWORK MODELS

All models can be deterministic or stochastic. The first models were deterministic, as illustrated by the orthogonal model by Snow (1965), which is defined by three orthogonal directions of equidistant planes. After this, models with purely random parameters were used, such as the Poisson flat process (Priest and Hudson, 1976), which presents the advantage of displaying many "good" properties. Stochastic models are considered here, because they are better adapted to usual applications. Their transposition to deterministic models is easy.

From a stochastic point of view, fracture networks are realizations of random sets. The basic models can be found among the random-set models, mainly developed by Matérn (1960), Matheron (1967, 1975), Miles (1972), and many others. Most models are reviewed by Serra (1982). Fractures are peculiar sets, because their third dimension is negligible with regard to the other two, so that they are considered here as planar. Therefore, the basic models of fracture networks are rather simple.

They will be described succinctly. A comprehensive description from a rock mechanics point of view can be found in Dershowitz (1984). A first presentation can be found in Chilès (1989a,b).

All the models described in this section share common assumptions:

i) All fractures are planar (assumption applicable to the whole chapter).

ii) All fracture locations are equally probable.

iii) All fracture orientations are independent of fracture locations.

However, the orientation is not necessarily uniformly distributed. This is even exceptional if directional sets are studied.

4.5.1 Infinite Fractures: Random Planes

In some cases, the fractures are long enough when compared to the studied domain, so that they can be considered as infinite. The simplest stochastic model is the Poisson flat model, defined by a single parameter λ and the following two properties:

i) if we consider the planes, whose poles lie within an elementary solid angle $d\omega$ centered on direction ω, their intersections with the line of direction ω that cuts across the origin of the coordinate system form a 1D Poisson process with density $\lambda\, d\omega$;

ii) the 1D Poisson processes induced along different directions are independent.

This model is obviously isotropic. A nonuniform distribution of fracture orientations can be achieved by replacing the constant density λ by a function $\lambda(\omega)$ of the orientation. Therefore, a simulation of Poisson flats within a ball of radius R can be achieved in two steps (Fig. 4.5.1):

i) simulation of a 1D Poisson process of density $\lambda_0 = \int \lambda(\omega)\, d\omega$;

ii) for each point of the Poisson process, selection of a random orientation according to the pdf $\lambda(\omega)/\lambda_0$; the corresponding random plane is the plane orthogonal to this orientation, whose algebraic distance to the origin is equal to the abscissa of the point of the 1D Poisson process.

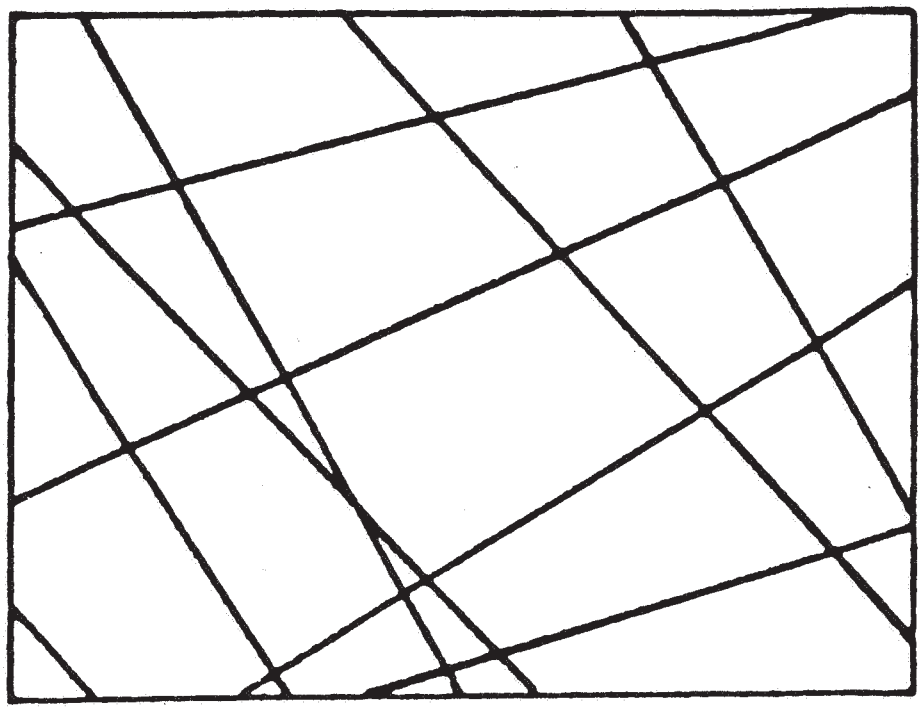

Figure 4.5.1. Section of a 3D model of random planes (Poisson flat process). After Chilès (1989a,b).

The simplicity of this model is very gratifying: ease of parameter fitting, availability of numerous properties of this kind of network through geometric probability theory (Kendall and Moran, 1963; Miles, 1969; Santalo, 1976). It is sometimes used in hydrological applications (see Andersson et al., 1984). The counterpart of this simplicity is lack of realism in most cases. Misuse of this model produces a too-systematic block network and an excessively connected fracture network.

4.5.2 Finite Fractures: Tessellation Models

Usually fractures are studied at a scale where they cannot be considered as infinite. Tessellation models give finite fractures. These models are built in two steps:

i) simulation of a set of jointed polygons, by partitioning of space or of fracture planes;

ii) selection, among these polygons, of those that will be considered as fractures.

The second step is achieved by randomly tossing for each polygon if it is a fracture (probability p) or intact rock (probability 1-p). The tosses are independent of each other. The probability p, or persistence, can be a function of the polygon orientation, in order to simulate anisotropic networks.

The first step can be achieved in several ways. The most commonly used in the present case are the following (Fig. 4.5.2):

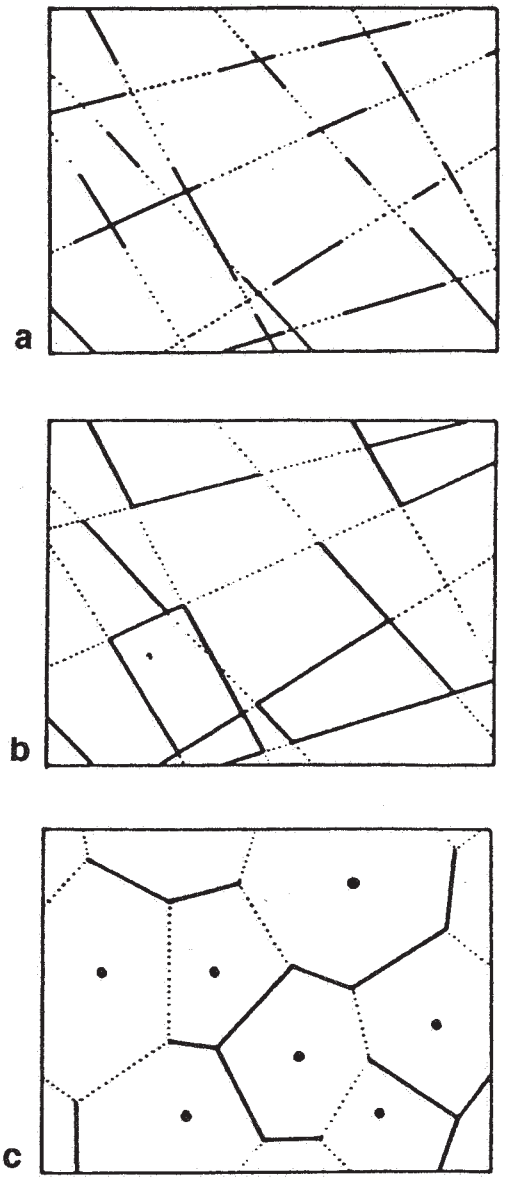

Figure 4.5.2. Section of 3D tessellation models: a) Veneziano model; b) Dershowitz model; c) Voronoï polyhedra. After Chilès (1989a,b).

a) tessellation of Poisson flats by Poisson lines: each Poisson flat is subdivided into Poisson polygons by an independent Poisson line process, which can be simulated with the same method as the Poisson flat process; this model was introduced for rock mechanics studies by Veneziano (1978);

b) tessellation of space by Poisson flats: a network of random planes already subdivides space into polyhedra, whose faces are polygons; fractures are chosen among these polygons. This model has been studied by Dershowitz (1984);

c) tessellation of space by Voronoï polyhedra: each point of a 3D Poisson point process (i.e., random points) is considered as the seed of a grain. Each seed grows at constant rate in all directions. Growth is stunted where two grains come into contact. This process subdivides the 3D space into polyhedra whose faces form a network of jointed polygons. Voronoï polyhedra and similar models (see Serra, 1982, Dershowitz and Einstein, 1988) enable us to model metallic grains, but are less suitable for rock fractures, with a few exceptions such as basalt pipes.

Each model corresponds to a different network type: Voronoï polyhedra produce noncoplanar fractures, whereas the other two models produce coplanar fractures. Fractures commonly stop when encountering another fracture in the Dershowitz model, whereas this never occurs in the Veneziano model.

The required fracture density and size are obtained by calibrating the Poisson density (of planes, lines, or points) and the persistence p. For example, Dershowitz reduces the polygon size by adding planes of zero persistence: no polygon of these planes is considered as a fracture, but these planes subdivide the polygons of the other planes. Persistence p has a strong influence on connectivity. In the first two models, where polygons are coplanar, each fracture is formed by one or several jointed polygons, so that the fracture size is a function of p.

4.5.3 Finite Fractures: Boolean Model of Random Discs

A Boolean model consists in the setting-up of a volumetric element at each point of a 3D Poisson process. This element can be the same all the time (for example, a ball of fixed radius r), or can be random (for example, a ball of radius r_i is set up at point x_i, where the r_i's are independent random variables with the same distribution). The definition and the general properties of Boolean models are due to Matheron (1967, 1975). For fracture networks, this model is used with a disc as the volumetric element, and is known as the random-disc model (Fig. 4.5.3).

It was introduced for rock mechanics applications by Baecher et al. (1977). Each fracture is assumed to be a circular (or elliptical) disc, and is defined by its central location, diameter and orientation. For this reason the model is defined by the following properties:

- the disc centers constitute a 3D Poisson point process;
- the disc diameters are independent and have the same distribution;
- the disc orientations are independent and have the same distribution;
- diameter and orientation are independent.

The last property may seem a limitation for the applications, but in practice a specific model is used for each fracture set. So, the fracture size can differ from one set to the other, whereas it is acceptable to consider that, within a set, size is independent of orientation. This model also has a limited number of parameters. They are directly related to the shape of the fractures.

The intersection of the network with a plane is a 2D model of segments centered on the points of a 2D Poisson process. The parameters of the 3D and 2D models (Poisson process densities, disc diameter and trace-length distributions) are related by simple stereological relationships (see Sec. 4.4.7). The 3D model parameters are hence easily deduced from 2D measurements.

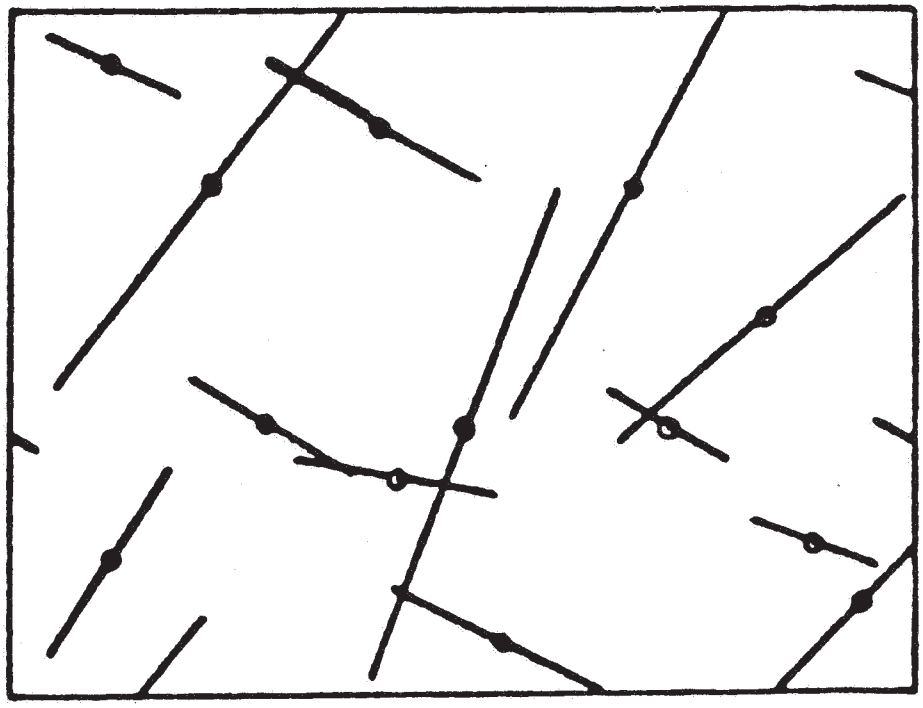

Figure 4.5.3. Section of a 3D random disc model. After Chilès (1989a,b).

In this model, blocks are only formed when fracture density or disc size is sufficiently high to cause intersections between triples of discs rather than pairs. Blocks are not shaped as convex polyhedra. Thus, this model seems suitable for rock masses that do not exhibit distinct rock blocks.

4.6 FRACTAL APPROACH

The fractal theory of Mandelbrot (1983) is now widely used in the earth sciences. Applications to fracture-network modeling are, however, not numerous, in spite of the kinship of the terms "fracture" and "fractal." The main parameter of fractal models is the fractal dimension.

4.6.1 Fractal Dimension – Box Dimension

The exact definition of fractal dimension, or Hausdorff dimension, does not provide a simple means of measuring it in a fracture network, but several alternative definitions exist that yield the same value as the Hausdorff dimension in the case of self-similar fractals. For fracture networks, the tool that is usually used is the box-counting dimension, or simply box dimension, initially called similarity dimension, as defined by Mandelbrot (1985).

To define this box dimension, suppose that we are studying a 2D pattern (a network of traces in our case). We can cover the study domain with a lattice made of square boxes of side r, and

count the number $N(r)$ of boxes that intersect the pattern (Fig. 4.6.1). If the pattern is a rectangle of area S and r is small enough, we have approximately $N(r) = S/r^2$. Likewise, if the pattern is reduced to a segment of length L parallel to one side of the boxes, we have $N(r) = L/r$. In both cases, the Euclidean dimension (2 or 1), is D so that $N(r)$ has the form $N(r) = A/r^D$, or equivalently:

$$\log N(r) = \alpha - D \log r$$

D, the box dimension, is the absolute value of the log-log plot slope of N versus r. This relation is generalized to more complex patterns, where D can be a non-integer value.

4.6.2 Scale Dependence

In practice, one must be very careful when analysing a log-log plot. The mechanical use of the method always provides a graph, even if the phenomenon is neither fractal nor self-similar. Of course, in this case the graph is not necessarily linear, but it may look approximately linear at the scale of the study. In the case of a fracture survey, the graph cannot be linear: for large r values, every box is intersected by one or several traces, leading to a global box dimension of 2; in the opposite case of very low r values, the local box dimension is 1, for the traces have been collected as segments. Of course this local dimension is obtained by using the data beyond their precision, but this shows that it is possible to get any box dimension value between 1 and 2, unless the scale, or more precisely the inner cut-off, is specified. This may explain why very dissimilar results have been presented: for example, Barton and Larsen (1985) found a dimension between 1.12 and 1.16 for three tuff outcrops; Jacquin and Adler (1987) gave a dimension of 1.8 to 1.9 to several fracture sets; Thomas (1987), with another method, concluded that the fractal behavior of several calcareous or granitic outcrops had a dimension slightly above 1. There are several ways to overcome these difficulties:

i) characterize the network by its whole box-dimension graph (the derivative of the log-log plot) instead of a single dimensional parameter (Chilès, 1988).

ii) specify the inner cut-off for which the local dimension is computed; Barton (1992) proposed to use as box cut-off the truncation length of the collected fractures; with such a

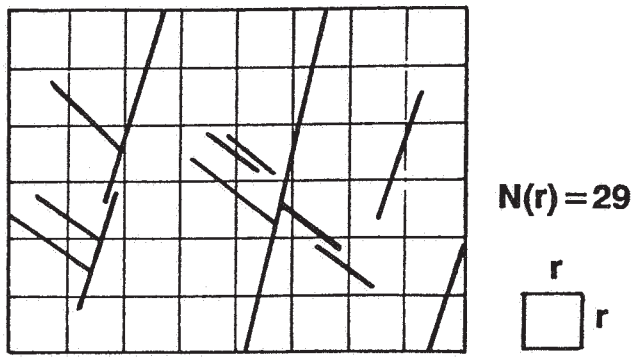

Figure 4.6.1. Definition of the box dimension. After Chilès (1989a).

definition, and also refinements in the computation of the box-dimension graph, he found a dimension between 1.6 and 1.8 for 15 different data sets, including the three tuff outcrops studied by Barton and Larsen (1985); the box-dimension graph of Chilès (1988) gives a dimension of 1.6 with Barton's definition of the inner cut-off.

iii) transpose to fracture networks other dimensional parameters, such as those developed for lattice models (see, e.g., Feder, 1988, Ch. 7).

4.6.3 Fractal Models

Even if the phenomenon is considered as fractal, the fractal dimension D itself yields no information on the model: D is simply the parameter of a model that must be chosen on the basis of other considerations. This is easy to understand if we compare the box dimension definition and the functional moment $Q(B)$ defined by Eq. (4.2.1) in the mathematical morphology approach: the knowledge of the box dimension graph is exactly equivalent to the knowledge of $Q(B)$ when B is a square box. This is not sufficient to fully characterize the network, as we know that it would require $Q(B)$ for any set B.

An exception is the 1D case (the fracture network is reduced to a network of points) when successive spacings can be considered as independent. This is why the few attempts to simulate a fracture network with a fractal model start from a 1D model: Thomas (1977) simulated infinite planar fractures from a fractal simulation of intersections with a sampling line. Chilès (1988) simulated finite fractures of fixed orientation and random length in a 2D case; the method takes account of the whole box dimension graph (Fig. 4.6.2). Barton (1992) combined fractal models (Cantor dust) and statistical characteristics (distribution of length and orientation) to provide a 2D simulation.

4.7 GEOSTATISTICAL APPROACH

The above basic models provide networks of independent fractures (random planes, random discs). These models are a good starting point for the study of actual fields. However, reality is often more complex, combining variable density, relays of fractures, and clusters. The geostatistical approach (Matheron, 1965) enables one to question, to validate, or, if necessary, to

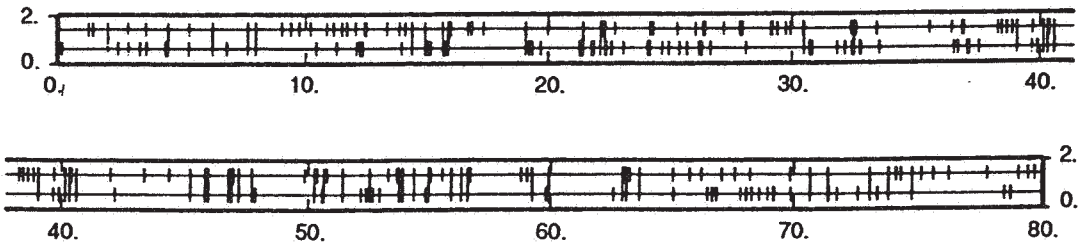

Figure 4.6.2. Simulation of a set of subvertical fracture traces on a 80-m by 2-m drift wall with a model reproducing a given box dimension graph. Only the intersections with two lines and the continuity are simulated. The distance between these two lines is equal to the mean trace length. The extension of the traces is conventional. After Chilès (1988).

weaken the assumptions of independence and of constant density that are the basis of these models. Among the first works on the subject see Miller (1979) and La Pointe (1980). For more recent developments refer to Chilès (1988, 1989a,b) and Massoud (1987).

Remember that the main geostatistical tool is the variogram. Considering a (random) function $Z(x)$, the variogram is the ordinary function of distance (or more precisely vector) h defined by

$$\gamma(h) = \text{mean}\,\tfrac{1}{2}\,[Z(x+h) - Z(x)]^2$$

It summarizes the dissimilarity of Z between two points at a distance h apart. The variogram is linked with the covariance function

$$C(h) = \text{mean}\,[Z(x) - m]\,[Z(x+h) - m]$$

where m is the mean value of Z, by the relation

$$\gamma(h) = C(0) - C(h).$$

4.7.1 Spacing

The intersection of any of the basic models with a line provides a 1D Poisson process. Successive spacings are independent and follow an exponential distribution (so that their relative variance equals 1). Instead of simply computing the mean spacing, it is worth verifying if the actual data satisfy these properties. This can be achieved by computing the experimental histogram and the variogram referenced to the fracture sequence number introduced by Miller (1979): the spacing values are not assigned to points on the sampling line, but to successive integer abscissae: the first observed spacing is assigned to the abscissa $x = 1$, the second one to $x = 2$, and so on. The h distance of variogram $\gamma(h)$ is then measured in number of fractures. For a Poisson process this variogram shows a pure nugget effect with sill equal to the square of the mean spacing.

Massoud (1987) for a granite massif, and Loiseau (1987) for gneiss, obtained flat variograms (pure nugget effect), but with a sill two to four times too high to correspond to a Poisson process. The histograms were obviously not exponential. Observation of fracture traces along drift walls shows that this is due to clustering. Fractures are grouped in clusters causing short spacing between fractures from the same cluster and long spacing when the two fractures belong to two distinct clusters. The same phenomenon was already observed by Snow (1970).

4.7.2 Fracture Trace Density

Another property of the Poisson process is that the number of points in disjointed segments (or volumes in space) are independent variables with a Poisson distribution. If we subdivide a surveying line into equal segments of length b and if, for distances $h = b, 2\,b, 3\,b, \ldots$, we compute the variogram of the number of intersections per segment, this variogram will also show a pure nugget effect. Its sill is equal to $d_1\,b$, where d_1 is the density of intersections with the surveying line. If a 2D survey is available, the surveyed zone can be subdivided into rectangles, and the same property holds for the variogram of the number of trace centers per rectangle; this is always

true for the random disc model, and approximately exact if the rectangle is large enough for the other models.

In the Fannay-Augères granite formation, most variograms computed by Massoud (1987) from 2-m-high drift wall surveys present:

- a nugget effect, corresponding to the random part of the fracture location;
- a first range of several meters, which may correspond to the extension of fracture clusters (increased by the regularization length b);
- longer-range components (30 to 300 meters), which can only be accounted for by a regionalized variation of the fracture density.

Loiseau (1987) found similar results in the Cézallier orthogneiss. La Pointe (1980) obtained ranges of about 80 m in dolomite.

4.7.3 Fracture Parameters

Other fracture parameters (orientation, size, thickness) can also be studied. The pole orientation within a set has been studied by many authors. La Pointe (1980) found an 80-m range in dolomite, Miller (1979) a 20-m range in granite, whereas Barla et al. (1987) in limestone and Massoud (1987) in granite, found ranges of several meters. In the latter case, this can be understood as the fact that fractures belonging to a cluster tend to have the same orientation, whereas cluster orientations are less correlated.

4.8 MORE GENERAL NETWORK MODELS

In order to take account of the complexity of reality, several simple generalizations of the basic models can be used.

4.8.1 Hierarchical Models

In their 2D study, Conrad and Jacquin (1973) observed long fractures and short ones that usually ended when encountering a long fracture, which led them to use a hierarchical model:

i) a primary network of infinite Poisson lines, that subdivides the plane into polygons;

ii) within each polygon, an independent process of random segments (the 2D version of the 3D random disc model); the segments are of course censored if they encounter the edge of the polygon (Fig. 4.8.1).

Another model is presented by Gervais et al. (1992). Such models are very useful for networks where a fracture set is stopped by another one.

4.8.2 Cluster Models

Models with fracture clusters are very simple. As all the basic models are based on Poisson point or flat processes, one has only to replace the Poisson process by a procedure in two steps:

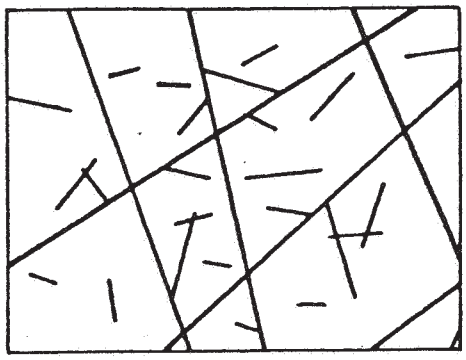

Figure 4.8.1. 2D hierarchical model of Conrad and Jacquin. After Chilès (1989a,b).

i) a Poisson process of lower density, which generates seeds (points or planes);

ii) around each seed, the generation of a cluster of independent points or planes (Fig. 4.8.2)

This kind of model has two new parameters: the mean number of elements of a cluster (the distribution of this number is difficult to determine, and thus a Poisson distribution is usually assumed) and the dispersion of the elements around the seed (for similar reasons, a Gaussian distribution is usually assumed). The density of seeds is taken as the ratio of the density of elements to the mean number of elements per cluster.

4.8.3 Regionalization of Density

If the fracture density is not constant, there are two ways to introduce a regionalization into the model, depending on the type of model:

i) for models based on Poisson points (Boolean model, Voronoï model), the density λ of disc centers can be replaced by a stationary random function $\lambda(x)$ with variogram $\gamma(h)$;

ii) for models based on Poisson flats, persistence p can be considered as a stationary random function (the randomization of the density of planes would introduce less flexibility).

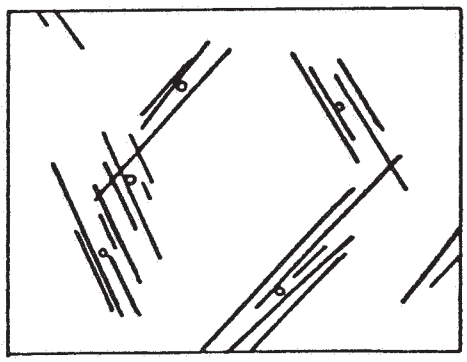

Figure 4.8.2. Section of a 3D model of disc clusters centered on Poisson seeds. After Chilès (1989a,b).

In this case, a parameter (e.g., the fracture density) is replaced by a distribution plus a variogram.

4.8.4 Parameter Fitting

These models are easy to simulate: regionalization can be achieved by a classical geostatistical simulation of the parameter (see e.g., Matheron, 1973; Mantoglou, 1987); mixed models and cluster models simply add one more step. The real problem is fitting the various additional parameters. In some cases, it is not more difficult than for the other parameters: for the 2D mixed models, Conrad used the functional moment $Q(B)$; for a model of Poisson twin flats, Matheron (1971) gave the spacing distribution of the twin planes from the distribution of the spacing of twin points that can be measured along a borehole, but usually the parameter fitting is more indirect. It can be carried out without major problems when the parameters of the model remain close to observable quantities. From this point of view, models of random planes or random discs offer much flexibility, as illustrated below for the latter.

4.8.5 Example of Disc Clusters with Regionalized Density

This is a rather complex model, as it generalizes the random disc model in two ways. Its parameters are the following:

- the cluster centers or seeds locally form a Poisson process of density $\lambda(x)$; this density is a stationary random function with mean λ and covariance $C(h)$;
- each cluster includes n discs; n is random, independent of all other clusters, and distributed according to a Poisson distribution with mean θ;
- the disc centers spread independently around the seeds according to a distribution with pdf $f(x)$ (usually an isotropic Gaussian distribution);
- all fractures of a cluster show the same orientation, but the cluster orientations are independent and have the same distribution;
- all disc diameters are independent and follow the same distribution, with pdf $h(D)$.

Orientation distribution, diameter distribution and average density of disc centers $\lambda\theta$ are determined for each studied fracture set as in the basic random disc model. Apart from complications due to a 3D modeling from 1D or 2D data, there are two difficulties in obtaining the other parameters:

- several clusters may overlap and it is not necessarily clear to which seed a fracture belongs; in this case, splitting the overall density $\lambda\theta$ into λ and θ is not easily done;
- the number of disc centers within a volume of size V centered at point x is not equal to the local density $\lambda(x)$ multiplied by θV, but to a realization of a random variable with mathematical expectation $\lambda(x)\ \theta V$; in this case the variogram of $\lambda(x)$ is not directly accessible.

When all parameters are fixed, it is possible to define the theoretical value of the variograms of fracture spacing and trace center number, which allows us to fit the remaining parameters by a trial and error method. The main theoretical results (Chilès, 1988, 1989a,b) are given below. Some demonstrations can be found in Massoud (1987).

The theoretical spacing variogram (or simply the relative spacing variance) is studied with a 1D Monte Carlo technique. This requires first the calculation of the distribution of the induced 1D clusters from the distribution of 3D clusters (not all fractures of a cluster intersect a straight line). If a fracture set orthogonal to the surveying line is considered, it is easy to demonstrate that the simultaneous 1D density of 1D clusters of m points that are part of a 3D cluster of n discs ($n \geq m$) is

$$\lambda_{mn} = \lambda \binom{m}{n} p_n \iint P(x,y)^m \, [1-P(x,y)]^{n-m} \, dx\,dy \qquad (0<m\leq n) \qquad (4.8.1)$$

We consider here a constant cluster density λ. The three coordinates x, y, z are explicit. The surveying line is the Oz axis; $p_n = e^{-\theta}\,\theta^n/n!$ is the marginal distribution of n; $P(x, y)$ is the probability for a disc of a seed located at point (x, y, z) to intersect the Oz axis. If the discs all have the same diameter D, one has:

$$P(x,y,D) = \iint C_D(-x,-y,0)\, f_1(u,v)\,du\,dv$$

but: $C_D = (-x,-y,0)$ shall be considered as an index

$f_1(u,v)\,du\,dv$ shall be in normal position:

$$P(x,y,D) = \iint_{C_D(-x,-y,0)} f_1(u,v)\,du\,dv$$

where $f_1(u, v)$ is the marginal pdf linked with pdf $f(u, v, w)$ of dispersion of disc centers around the seeds, where $C_D(-x, -y, 0)$ is the disc of diameter D centered on point $(-x, -y, 0)$.

Randomizing D, one gets:

$$P(x,y) = \int P(x,y,D)\,h(D)\,dD$$

The marginal density of 1D clusters of n points is then

$$\lambda'_m = \sum_{n\geq m} \lambda_{mn}$$

Figure 4.8.3 presents the relative standard deviation of fracture spacing as a function of the mean number of discs θ for several values of the dispersion (the pdf f is assumed to be isotropic Gaussian, and is characterized by its standard deviation). This makes a good evaluation of θ possible if the dispersion of a cluster is not too high. If the fractures are not normal to the surveying line, but intersect it at an acute angle β that remains close to $\pi/2$, these results remain

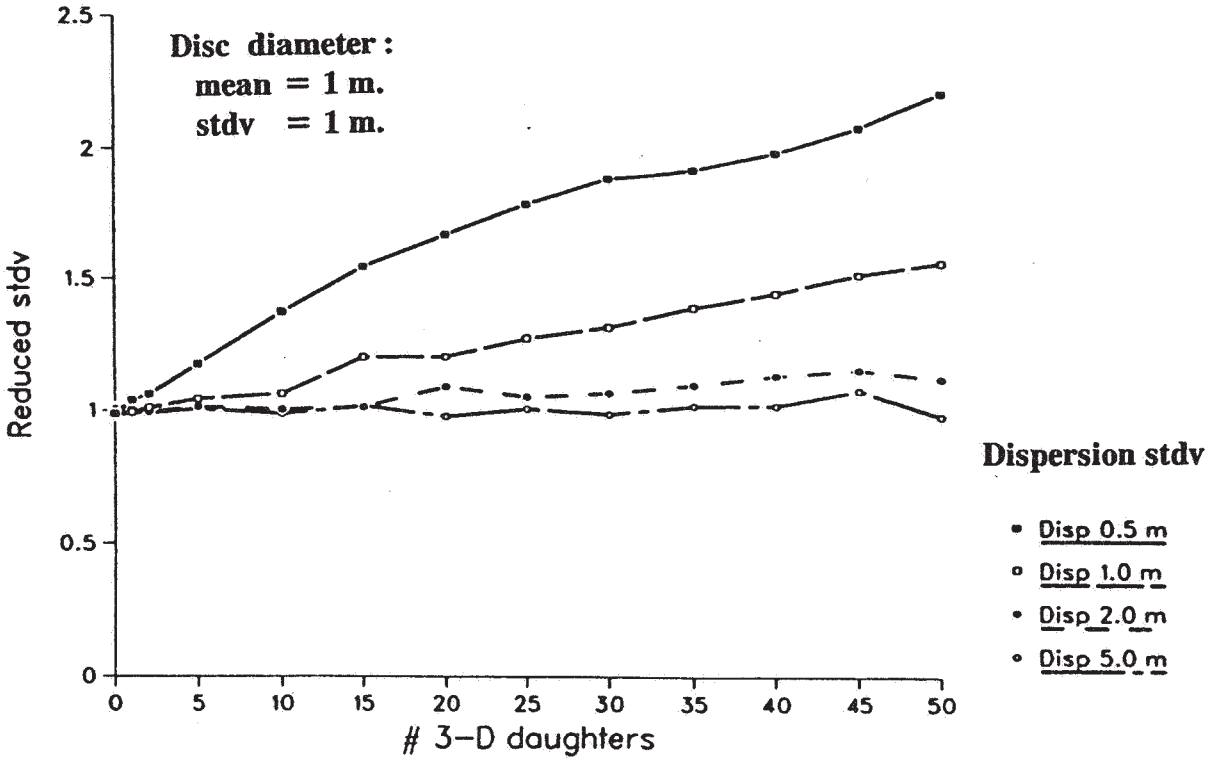

Figure 4.8.3. Theoretical relative standard deviation of fracture spacing for a model of disc clusters, as a function of the average number of discs per 3D cluster, for various dispersions of the disc centers. The disc diameters are lognormal with mean = 1 m and standard deviation = 1 m. After Chilès (1989a,b).

valid in a first approximation, provided that $P(x, y, D)$ is replaced by $P(x, y, D \sin \beta)$ in the expression of $P(x, y)$. If the density λ is not constant, the experimental relative variance must be computed locally.

The derivation of the theoretical variogram of the trace center number is explained in Massoud (1987) and Billaux et al. (1989). Figure 4.8.4 presents this variogram for several sets of parameters. If θ is known, a good evaluation of the dispersion of the disc centers and of the variogram $\gamma(h)$ of the density $\lambda(x)$ can be made.

The detailed application of this method to actual data collected in the Fanay granitic site is described in Massoud (1987) and Billaux et al. (1989).

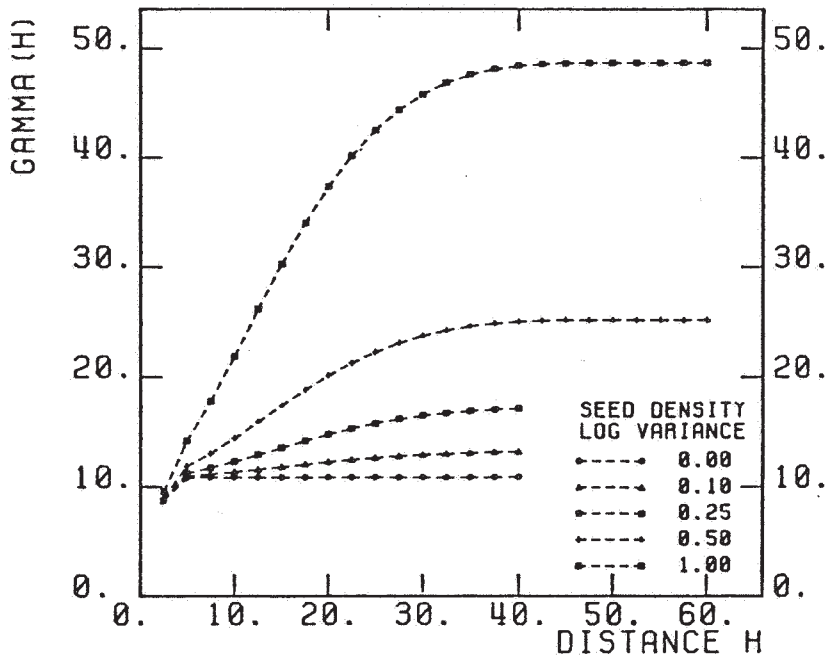

Figure 4.8.4. Theoretical variogram of trace center number for a regionalized model of disc clusters, for various variances of the seed density. The seed density is lognormal; its logarithm has a cubic variogram with a range of 50 m. The average seed density is 0.05 par m^3, and the average number of discs per 3D cluster is 20. The disc diameters are lognormal with mean = 1 m and standard deviation = 1 m. After Chilès (1989a,b).

4.9 CONDITIONING TO THE DATA

The tools examined above allow the fitting of all the parameters of the chosen 3D model from 1D or 2D data, and the simulation of a 3D fracture network that has the same statistical properties as the actual network. However, it would be even better if the simulated network also coincided with the actual network at the location of the 1D or 2D data.

4.9.1 Conditioning to Fracture Density

Seismic tomography methods are improving. They can at least give the relative variations of the fracture density between two boreholes, and define the precision of the method. These new data can be used to condition the simulation of fracture density in a model with regionalized density. The conditional simulation of random functions is well-known in geostatistics (e.g., Delhomme, 1978, 1979).

4.9.2 Conditioning to Observed Fractures

Conditioning to observed fractures can be easily made for models directly based on Poisson processes because all points, lines, or flats of a Poisson process are independent of each other. Thus the general outline of a conditioning is as follows (Fig. 4.9.1):

1. produce a nonconditional simulation;
2. reject all the fractures that intersect the surveyed lines or surfaces, and retain all those that do not intersect;
3. add the actual fractures that have been surveyed.

The simplest case is the Poisson flat model because fractures are infinite. This model was used by Andersson et al. (1984). For a random disc model (see e.g. Andersson and Dverstorp, 1987), step 3 introduces a slight complication because the extension of the fracture must be determined from an intersection or a trace; in other words, we need the joint distribution of disc diameter and disc center location conditioned by observation (point or trace length). This results from geometric probability calculations. Such a simulation, based on actual data, is presented by Chilès et al. (1992).

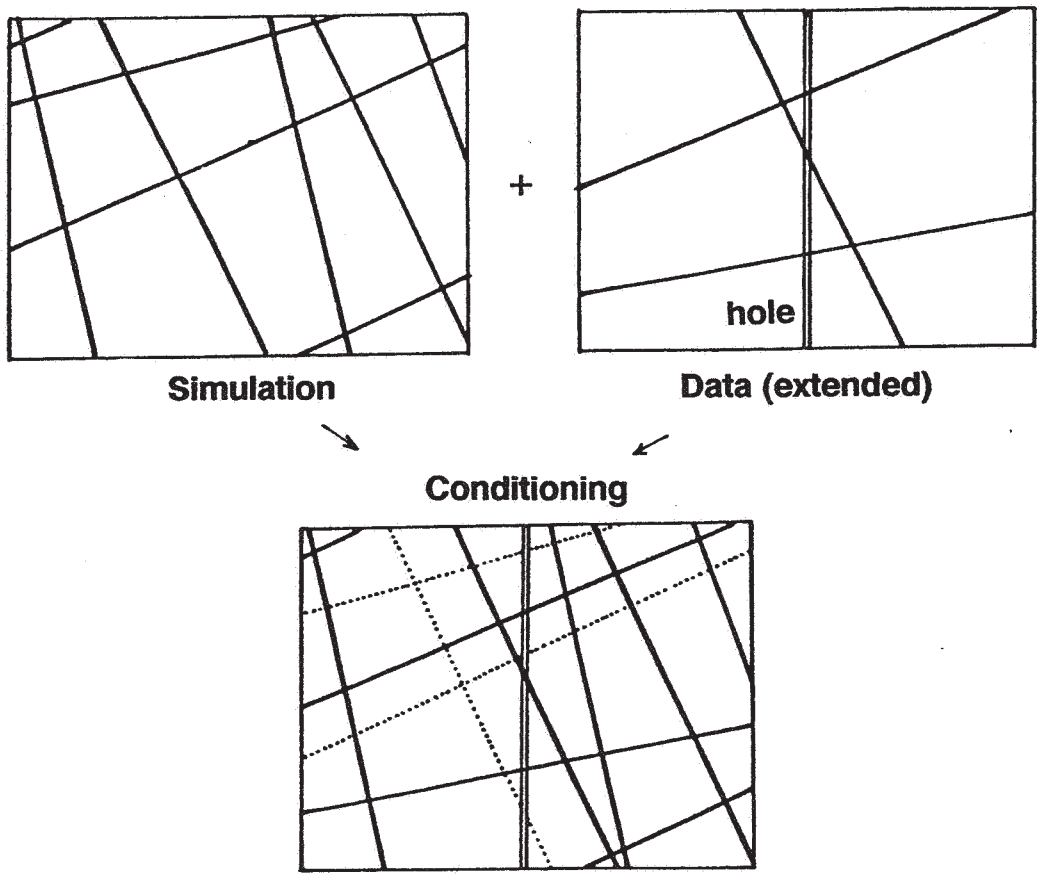

Figure 4.9.1. Conditioning of a simulation of random planes to borehole data. After Chilès (1989a,b).

With a disc cluster model, the same approach can be used (Chilès, 1989a,b), but, because independence is now at the cluster level, the rejection defined in step 2 must be applied at this level: we must reject all the fractures of the cluster as soon as one of them intersects the surveyed lines or surfaces. Conversely, in step 3, we must add to the surveyed fractures a simulation of the other fractures belonging to the same clusters (Fig. 4.9.2).

To achieve this, we need the distribution of the total number n of discs of a cluster conditioned by the number m of visible discs of the cluster. In the case of borehole data, this conditional distribution derives directly from the joint distribution of m, n, x, y that is the basis of expression (4.8.1) of λ_{mn}. The location of disc centers and their diameters are simulated from their a priori distributions by means of an acceptance/rejection technique. Thus, the theoretical tools are available. The main constraint is practical: the user must be able to define from the data which fractures belong to the same cluster; but this can usually be done with a good confidence.

4.10 CORRELATION BETWEEN SETS

The various directional fracture sets are usually studied independently but in fact, these sets are often found at correlated locations. Negative correlations (competition effect: recent tectonic

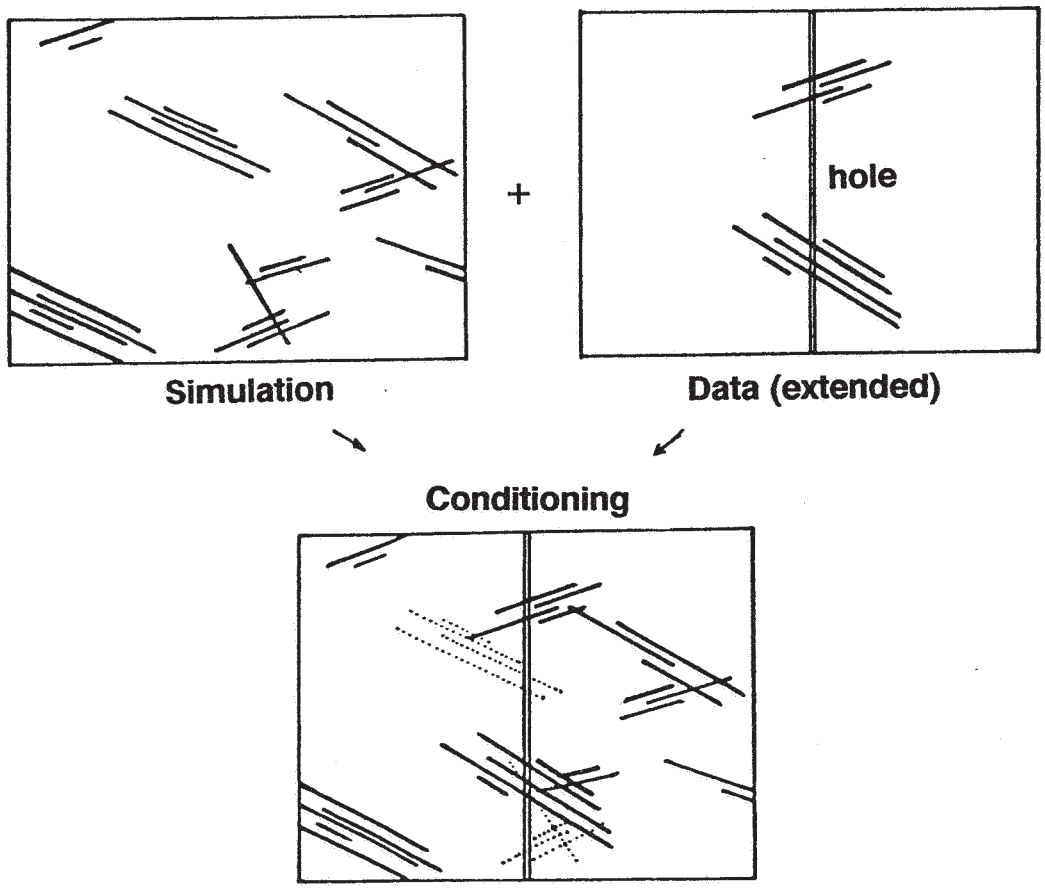

Figure 4.9.2. Conditioning of a simulation of disc clusters to borehole data. After Chilès (1989a,b).

episodes open new fractures in previously nonfractured areas only) as well as positive correlations (conjugate sets, zones of weakness in rock; e.g., Loiseau, 1987) can be observed. It is important to take these correlations into account because of their impact on connectivity. This can be done, for example, by means of correlated fracture densities.

4.11 THE SINGLE FRACTURE

If the fractures are considered as discs or polygons of constant aperture, it is possible to perform 2D flow calculations on the whole fracture surface, but actual fractures have nothing in common with perfect pairs of parallel plates. It is therefore necessary to use models that take account of the actual shape of fractures. Two approaches are possible:

i) A global approach to the single fracture: the flow and transport properties of a fracture are summarized by a few parameters. These parameters, or their distributions, are fitted by means of hydraulic tests.

ii) A local approach to the single fracture: the topography of the fracture walls and the induced aperture are modeled by (random) functions. This can be the basis for a representation of the void space by channels or conductive pipes, from which flow and transport calculations are performed.

4.11.1 Global Approach to the Single Fracture

Cacas (1989) and Cacas et al. (1990a) characterized each fracture by a mean hydraulic head. Flow between secant fractures is summarized by a 1D hydraulic link where flow rate is proportional to the head difference between the two fractures. The ratio of flow rate to head gradient is defined as the integrated hydraulic conductivity. This parameter represents the average resistance to flow between the two fractures and integrates the entire flow geometry: surface roughness, flow tortuosity, and channeling. The distribution of the integrated conductivity specifies the hydraulic model. A lognormal distribution is usually used, and its parameters are determined by trial and error from hydraulic tests in order for the model properties to correspond to the observed ones. The network of linear links replaces the network of discs. Flow and head are computed by using Kirchhoff's law. (See Sec. 4.14.)

Cacas (1989) and Cacas et al. (1990b) studied the particle transport with a particle-following method. Two parameters summarize the properties of the fractures: i) the retardation coefficient, related to the channel shape; and ii) the microscopic dispersivity, linked with dispersion phenomena within the fracture planes. (See Sec. 4.15.)

4.11.2 Geostatistical Modeling of the Single Fracture

The precise shape of a fracture can be studied at the laboratory scale on a core orthogonal to the average fracture plane. Measurements can be made by sampling profiles along both fracture walls (Gentier, 1986), or by analyzing the image of a translucent cast of the void (Billaux, 1990). The latter method offers the advantage of a complete description of the aperture, but gives no information concerning the shape of the fracture walls. The translucent cast data are sufficient for

flow studies. For transport and mechanical studies, however, it is necessary to also consider the fracture wall profiles.

A fractal approach, combined with spectral analysis, was used by Mandelbrot et al. (1984) in the study of a metal fracture surface, considered as a fractional Brownian surface. Brown and Scholz (1985) used a fractal approach for the study of natural rock surfaces. A geostatistical approach seems preferable for two reasons: i) it includes a wider class of phenomena than the fractional Brownian model, which simply corresponds to intrinsic random functions with an h^{α} variogram; and ii) it enables the user to analyze simultaneously the shape of the fracture and the relationship between walls and aperture.

Gentier (1986) presents the variography of an actual fracture surface. Gentier et al. (1991) simultaneously analyze the topography and the gradient in order to ensure a good modeling of the roughness. But let us examine a very simple example of the usefulness of a simultaneous study of walls and aperture.

Denoting the 2D coordinates as x in the average fracture plane and the axis orthogonal to this plane as z, the elevations of the lower and upper fracture walls are represented by two functions $Z_1(x)$ and $Z_2(x)$. The aperture is then the function $Z_3(x) = Z_2(x) - Z_1(x)$. The walls Z_1 and Z_2 are often similar. Due to all these relations, Z_1, Z_2 and Z_3 are not independent.

Suppose that the two walls are identical, up to a displacement. Then one has:

$$Z_1(x) = Z(x) \qquad Z_2(x) = b + Z(x + a) \qquad Z_3(x) = b + Z(x + a) - Z(x)$$

where b is the average aperture (vertical displacement), and a is the translation (horizontal displacement). Denoting $C(h)$ the covariance of both walls and $\gamma(h) = C(0) - C(h)$ their variogram, such a displacement is easily detected on the wall cross-covariance, as $C_{12}(h) = C(h + a)$ is translated from $C(h)$, with its maximum for $h = a$ instead of $h = 0$. This displacement can also be detected on the aperture variogram $\gamma_{33}(h)$, as it is easy to see that:

$$\gamma_{33}(h) = 2\,\gamma(a) + 2\,\gamma(h) - \gamma(h - a) - \gamma(h + a)$$

When $h >> a$, $\gamma(h)$ can usually be considered as linear between $h - a$ and $h + a$, so that $\gamma_{33}(h)$ is at its sill $2\gamma(a)$. Figure 4.11.1 represents the aperture variogram $\gamma_{33}(h)$ linked with a linear wall variogram $\gamma(h)$. Along the translation direction, it has a range equal to the translation a. Its behavior below this range is also linear, but with twice the slope of the wall variogram. Along other directions, the behavior is similar, but with a smoother transition to the sill. This kind of variogram can be found on actual fractures. More complex phenomena can be studied in a similar fashion (Chilès and Gentier, 1992). The aperture variogram is more characteristic of the movement that created the fracture than of the topography of the fracture walls, so that its study is very useful from the point of view of the structural geology.

4.11.3 Channeling of the Single Fracture

When the value of the aperture is known at any point — from a void cast or from an interpolation of profile data — it is theoretically possible to calculate flow by assigning to any point a transmissivity as a function of the aperture and then using a finite differences model. This method would be very cumbersome and, in fact, is not suitable since the aperture is much smaller under stress than that measured on the void cast. Gentier (1986) and other authors have observed

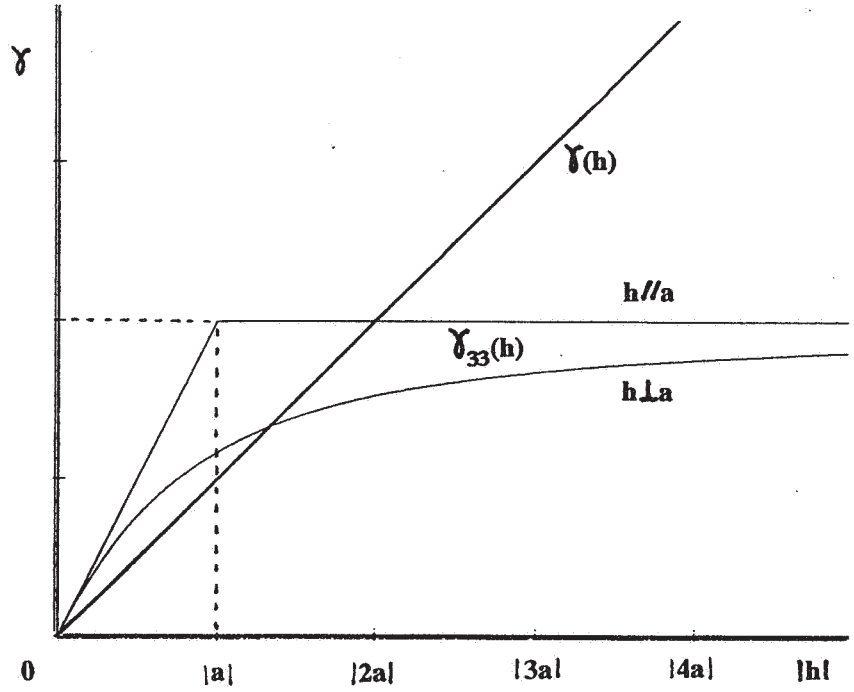

Figure 4.11.1. Aperture variogram linked with a linear variogram for the fracture walls, and a translation a along the Ox axis.

that, under stress, the water flow is usually along channels. Hence the idea, from the flow-studies point of view, of representing each fracture by a network of channels or conducting pipes. The approach can be global, in the sense that each fracture is replaced by a 2D network of Poisson lines or of Boolean random segments with a priori given parameters (Billaux, 1989). However, a model based on the observation of actual fractures is much better. This approach has been used by Billaux (1990) on a void cast. Figure 4.11.2 presents the successive main steps of the treatment: i) threshold at a given aperture value, visualizing the contact and void areas under normal stress (Fig. 4.11.2.a); ii) morphological skeletonization, followed by a suppression of dead ends and small loops, reducing the void areas to a network of channels (Fig. 4.11.2.b); and iii) reduction to a network of nodes and linear links (Fig. 4.11.2.c). The skeletonization is performed in such a way as to associate with each skeleton point the area of the corresponding channel cross-section. The flow calculation within the fracture is computed on this network. In this example, the diameter of the core is 11 cm. It is of course not useful, for a study at the 100-m scale, to model the precise fracture shape at the millimetric scale, and these results have to be transposed at least to the scale of the whole fracture.

4.12 FROM FRACTURE SYSTEM GEOMETRY TO CONNECTIVITY AND FLOW

If every fracture or fracture intersection is associated with a hydraulic parameter or if every fracture is replaced by a network of channels with given parameters, it is possible to compute the water flow through the network (see Cacas, 1989; Cacas et al. 1990a; Billaux, 1989). However,

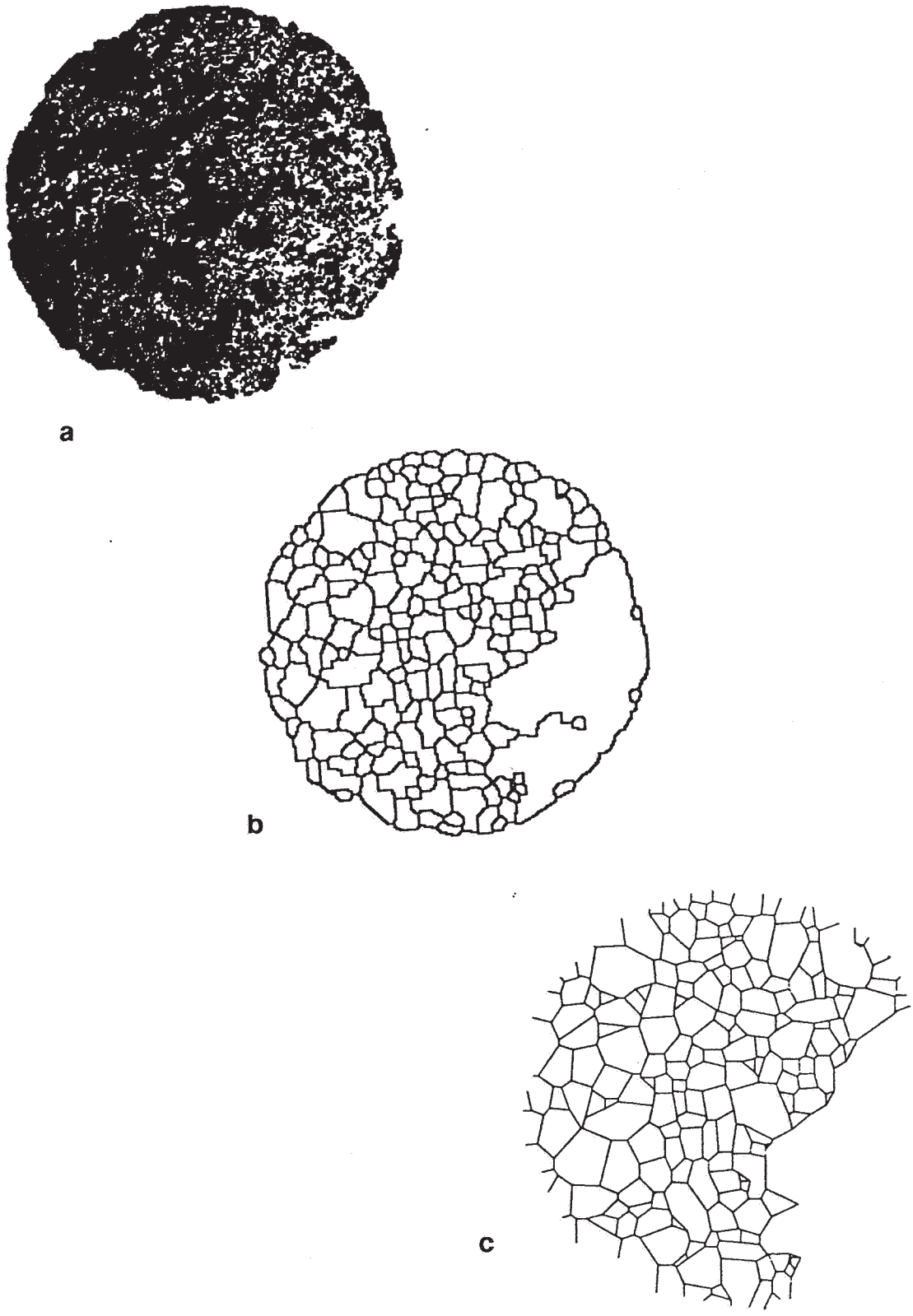

Figure 4.11.2. Representation of a single fracture by linear channels: a) binary image at a given threshold, visualizing the contact and void areas under normal stress; b) skeleton (after suppression of dead ends and small loops); c) network of linear channels. After Billaux (1990).

as actual fracture systems are complex, this requires long calculations. But flow is related to connectivity: if the fractures are not connected or form small separate clusters, no flow is possible whereas, if the fractures are highly connected, the system behaves like a continuous medium. As it is simpler to compute connectivity than flow, the connectivity can be studied first, in order to avoid flow calculations when they are not necessary.

Billaux (1989) presents a numerical example of hydraulic tests, injections with constant flow at the central hole of a simulated channel network, and prescribed head at the limits. Two curves are computed for each of six simulated networks: i) the connectivity curve, defined as the number of points of the channel network that can be reached from the injection point as a function of the distance to the injection point; and ii) the hydraulic head at the injection point as a function of time. The study shows that the shape of the head curve is very well explained by the shape of the connectivity curve. This is true not only in the extreme cases of very low or very high connectivity but also in the intermediate cases. A very interesting example is presented in Fig. 4.12.1. It corresponds to a network that seems to be near the percolation threshold. Figures 4.12.1a and 4.12.1b display the two steps of the network simulation: i) simulation of random discs; and ii) simulation of channels (intersections of discs, plus random segments on each disc). Figures 4.12.1c and 4.12.1d present the connectivity and head curves, which are rather regular and express a fairly good connectivity. This field is, however, far from being perfectly connected in three dimensions. It is easy to see that in the case of a 3D continuous medium that is perfectly connected connectivity varies as the square of the distance. This would lead to a slope of 2 on a log-log plot such as in Fig. 4.12.1c. Similarly, for a 2D continuous medium, this slope would be equal to 1. The corresponding lines are shown in Fig. 4.12.1c. The actual slope is around 0.66 (the first part of the curve should not be taken into consideration, as it is too dependent on the precise location of the injection hole). Thus, the actual network is less connected than a 2D continuous medium. If the notion of dimension of a continuous medium is extended to noninteger values, the analogy with the 2D and 3D cases shows that the slope of the log-log plot is equal to the dimension, minus 1. In the present case, the network can be considered as an equivalent continuous medium of dimension 1.66. The lack of connections produces a deficit in dimension in comparison with the Euclidean dimension of the whole space (3 in this example). This result can be compared with fractal concepts. Barker (1988) has derived the analytical expression of flow in the case of a medium with a noninteger dimension. Hence, the characterization of the connectivity of a network should give access to a simple model of its hydraulic behavior. A numerical example is given by Billaux (1990).

Another approach was explored by Hestir and Long (1990). They determined how a 2D network of random segments can be considered as equivalent to a regular lattice of bonds. This makes it possible to apply to random networks the results available for lattice networks. In particular, the correlation length can be derived from the percolation theory, which leads to a theory for the size of the representative elementary volume.

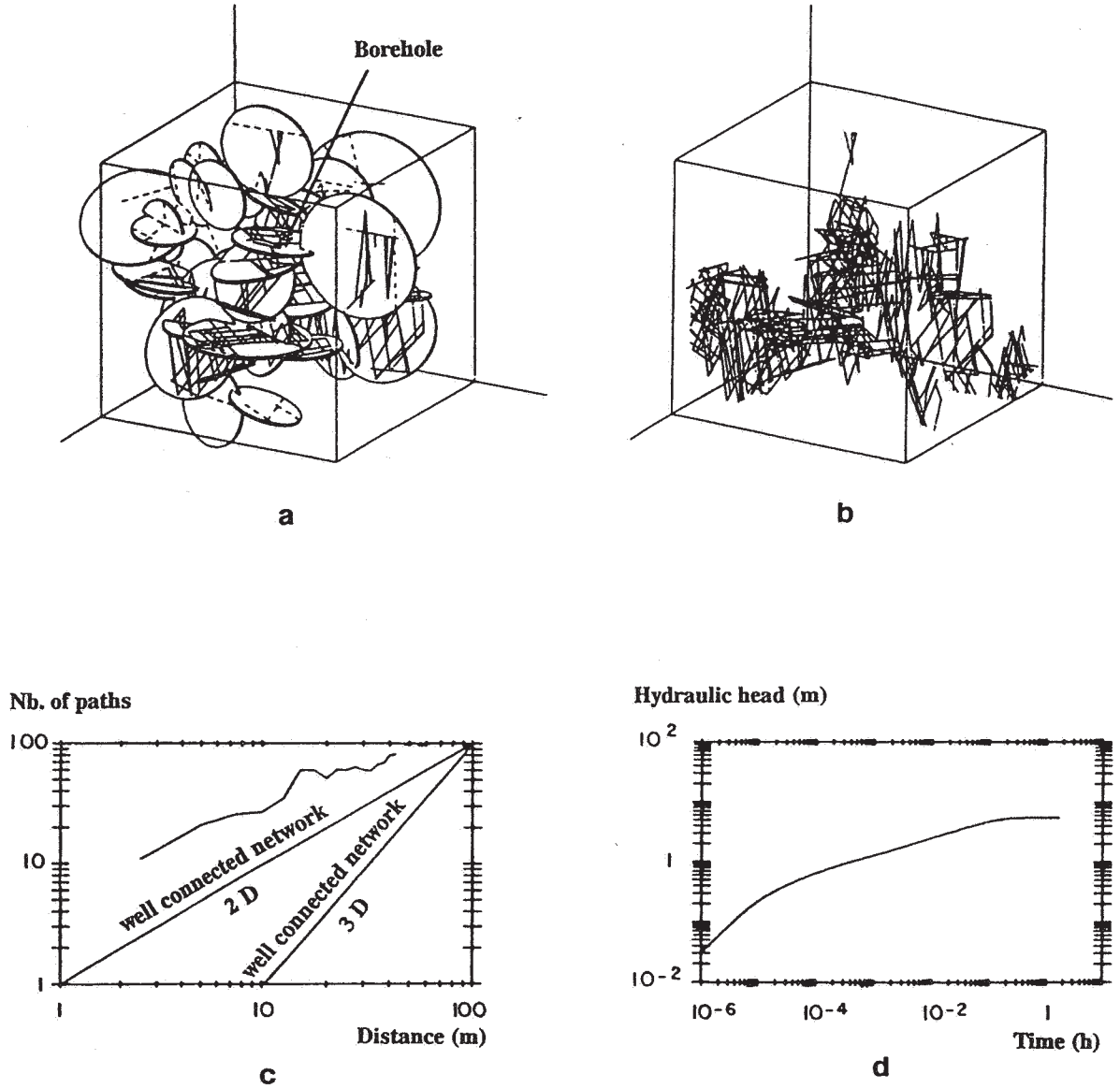

Figure 4.12.1. Connectivity and flow: a) network of random discs; b) network of channels; c) connectivity curve; d) head curve. After Billaux (1989).

4.13 PERCOLATION THEORY AND CONNECTIVITY

4.13.1 Definition of the Percolation Threshold

As stated in Sec. 4.12, a rock mass made of an impervious matrix and with a network of open fractures will only conduct water at a large scale if the fractures intersect; if one imagines that the density and/or length of the fractures in a network is progressively decreased, the connectivity of the network will also decrease; at a given density/length, the fractures, on average, no longer connect, and the rock mass becomes globally impervious. It may, however, happen that a small number of fractures in the network are still connected, in which case the network may be locally pervious: one may, for instance, inject water into one borehole and recover it in another one, provided that both boreholes belong to the same local set of connected fractures. If they belong to different local sets of connected fractures, no water can flow from one borehole to the next. It seems that such behavior can be observed in reality in some crystalline rocks (Marsily, 1985).

This problem of connectivity has already been addressed in other branches of physics, e.g., clogging of a filter, breaking of an electric circuit, and semi-conductor physics. A general mathematical theory for treating such issues, the "percolation theory," was proposed in 1957 by Broadbent and Hammersley (e.g., see also Shante and Kirkpatrick, 1971; Kirkpatrick, 1975; Clerc et al, 1983). In a network of increasing connectivity (starting from a low density/short length of the fractures without global connectivity), the local sets of connected fractures are called "finite clusters," and the sudden birth of a global permeability is said to happen at the "percolation threshold." At this threshold, one of the finite clusters becomes infinite: the medium is globally pervious; but local finite clusters may still exist together with the infinite one, at least when the network remains above, but close to, the percolation threshold.

Theoretical work as well as major numerical experiments have been carried out to determine, in general, the value of the percolation threshold in 2 or 3 dimensions as a function of the properties of the network as well as the conductive properties of the network in the vicinity of the percolation threshold (e.g., see Clerc et al., 1983).

It is therefore of interest to draw on these existing results for fracture networks. A first concept that emerges is the existence of a threshold in fracture conductivity; until recently, hydrogeologists considered fracture flow only as a scale problem: it was impossible to describe locally the flow in fractured media with continuum mechanics, but if a large enough "representative elementary volume" could be defined, any fractured medium ought, at that scale, to obey the flow equations of an (anisotropic) continuous medium. The only question was "how large is large enough?" and how to determine the large-scale hydraulic conductivity tensor (we will address these issues in Sec. 4.15). Percolation theory tells us that, before we attempt to answer such questions, we have to determine if the network is at all connected, i.e. whether it is above the percolation threshold. If not, the concept of "representative elementary volume" is useless and the global permeability is zero.

One must, however, strongly emphasize here that when one deals with fracture flow, the fractures that should be considered in any analysis are those that are pervious, at least locally (if channeling occurs): any crack or fracture that is totally sealed by, for example, calcite, silica, or clay, or is completely closed by the stress field plays no role or a very small one in fracture flow. The fractures that are observed in purely geometrical descriptions of the medium, e.g., from the observation of outcrops, or of drift walls or cores, are not necessarily those that conduct water. In fact it has been shown (e.g., see Ch. 2) that often less than 20% of the total number of fractures

are water-conducting. It is very difficult in practice to determine which fractures are water-conducting; it is therefore common to initially consider all the fractures of the medium, whether sealed or not, and then to randomly suppress a certain number (e.g., 50% or 80%) in order to represent the remaining water-conducting network. The number of fractures to eliminate is then a parameter of the model that can be calibrated (perhaps fracture set by fracture set) or, possibly, estimated from observation of the ratio of "dry" fractures to "wet" fractures on outcrops. We will show in Sec. 4.14.2 and 4.14.3 how this calibration can be done, and how a logical order of fracture aperture or conductivity can be used to select the fractures to eliminate from the initial network.

A second useful procedure is to try to determine the value of the percolation threshold from some properties of the medium. Intuitively, one expects these properties to be the density and the length of the fractures or the average number of intersections of any given fracture with its neighbors. It can be shown that this is indeed the case. It is, however, necessary to first make sure that random stochastic fracture networks are a class of objects similar to the other networks studied in physics, such as electrical networks. This has been done, for example by Vere-Jones (1977), Chelidze (1982), Dienes (1982), Robinson (1984), Engelman et al. (1983), Robinson (1984), Guyon et al. (1984), and Wilke et al. (1985), and applies in principle to purely random Boolean sets of discs (i.e., not for discs structured in directional sets of fractures); it gives, however, only approximate values for the percolation threshold. One finds (Robinson, 1984; Charlaix et al., 1984; de Marsily, 1985) that:

i) in 2D (network of lines of random orientation and random finite length) Robinson showed that the average number of intersections of any fracture with all other fractures of the network must lie between 3.2 and 3.8 at the percolation threshold. Alternatively, the dimensionless number p

$$p = d \times r^2$$

must be on the order of 1.5 at the percolation threshold, where d is the density of the network (number of lines per unit area) and r the average length of the lines. If the orientation of the lines is not purely random, i.e., structured into families, the threshold is slightly larger than 1.5.

ii) in 3D (which is the only realistic case, the 2D case is only of academic interest) Charlaix et al. proposed that for a random network of fracture planes, the dimensionless number p

$$p = d \times (\text{average area of the fractures}) \times (\text{average half perimeter})$$

must lie between 1.5 and 3 at the percolation threshold, where d is again the density (number of fractures per unit volume of rock). If the fractures are circular discs, the average area of the fractures and the half perimeter are functions of the radius; the percolation threshold is then obtained when

$$p = d \times (\text{average of the square of radius}) \times (\text{average of radius})$$

lies between 0.15 and 0.3; if all the fractures have the same constant radius r, then this product is just

$$p = d \times r^3$$

4.13.2 Properties of the Network in the Vicinity of the Percolation Threshold

Apart from the definition and estimation of the percolation threshold, the percolation theory is also able to describe some fundamental properties of networks in the vicinity of this threshold. The power of the theory lies in the fact that the properties of the network at a large scale are not related to its local geometry or configuration but to general properties of connectivity, which are independent of the actual network of interest and can be addressed generally; "universal constants" can thus be determined. For instance :

i) below the percolation threshold, the "correlation length," i.e., the average size of a finite cluster, is given by :

$$X(p) = A\ \varepsilon^{-\nu}$$

ii) above percolation threshold, the conductivity is given by:

$$K(p) = B\ \varepsilon^{\tau}$$

where A and B are constants (that depend on the particular network of interest), $\varepsilon = p - pc$ is the "distance" of the network to the percolation threshold, p is the dimensionless number defined in Sec. 4.13.1, and pc is the value of this dimensionless number at the percolation threshold. ν and τ are "universal constants" that are approximately independent of the network. Clerc et al. (1983) provide the following values :

	2D	3D
ν	1.33	0.89
τ	1.00	1.75

Such results may be useful for sensitivity studies, e.g., to determine how the hydraulic conductivity of a fracture network would vary if the density or size of the fractures were varied. They can be used even without building a stochastic model of the fracture network. They are, however, only approximate.

4.14 USE OF STOCHASTIC FRACTURE NETWORK MODELS FOR FLOW PROBLEMS

In sections 4.5 to 4.10, it has been shown how geometric stochastic discrete fracture network models can be built in three dimensions from geometric information on the fracture system; in sections 4.12 and 4.13, the connectivity of this fracture network was discussed, as it is of overwhelming importance in understanding and simulating fracture flow. In section 4.12, it was also shown that it is difficult to actually measure the apertures of the fractures in the field, and therefore that this parameter has to be determined differently. In this section, we will review how the geometric fracture model can be built into a flow model and how this model can be used.

4.14.1 Building the Flow Model

Most discrete fracture flow models have, so far, assumed that the flow in the domain is laminar, i.e., a linear relationship can be found between flow and hydraulic head gradients. Only Bruel (1990) extended that approach, by an iterative technique, to the case where the opening of the fracture is a function of the pressure within it, and coupled a mechanical discrete network model to a flow model to calculate the change in opening due to the pressure field. The flow is still assumed laminar, but the flow equations are no longer linear, because the hydraulic conductivity is a function of the aperture of the fractures. For a presentation of nonlaminar flow in fractures, see for example Louis (1974), or de Marsily (1986).

So far, four approaches have been used to solve the linear flow equations in the fracture network.

i) Analytical expression. In this first approach, the flow in each fracture plane is calculated assuming that the whole surface of each fracture is the flow domain. If the fracture is a smooth parallel plane model of constant aperture, it is possible to develop an analytical expression for the flow in each fracture plane (Long, 1983). Using the image theory in a bounded circular geometry, Long developed a steady-state expression that relates the head along a line in the fracture plane to the flow within the fracture, given the geometry of that line and the aperture of the fracture. Of course, for flow to occur in steady state in a fracture plane, at least two lines must lie along each fracture plane: these lines represent the intersections of the fracture planes with other fractures (Fig. 4.14.1). The solution is approximate in that the head along each line is assumed constant over its length, whereas, in reality, it might vary with position. This head therefore represents an average head along each intersection and is common to two intersecting fractures. More than two intersections for any given fracture plane can of course be considered.

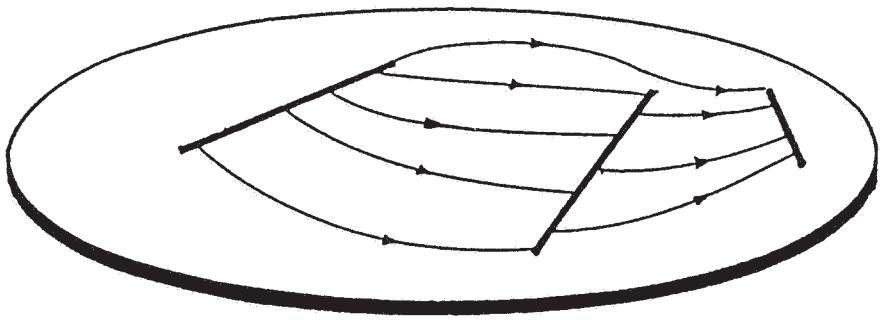

Figure 4.14.1. Flow between two parallel plates in a disc-shaped fracture with three intersections. After Cacas (1989).

For each fracture plane the analytical solutions provide the values of the flow entering or leaving that fracture plane at a given intersection, in the form of a linear function of the values of the heads along each intersection of that particular plane. Assembling these local flow models to form the global network model is then trivial, at least in principle. In steady state, at any given intersection of two fractures, the algebraic flow entering or leaving one fracture of the intersection must equal the negative of that calculated for the second fracture. This gives as many linear equations as there are intersections with just as many unknowns, which are the values of the heads at these intersections. This is known as a Kirchhoff problem in electricity or in pipe-network analysis, and it is simply the application of the principle of mass balance, assuming that the water compressibility can be neglected. Alternatively, the flow at the intersections can be the unknowns, and the heads, calculated as a linear function of the flows at the intersection, are made equal for each of the two intersecting planes.

The boundary conditions can be a prescribed head at any given intersection (e.g., when a fracture outcrops), thus reducing by one the number of equations and unknowns; a no-flow condition is simply represented by not allowing flow to occur through a given intersection, i.e., removing it from the given fracture plane. Source terms can be added if necessary at any intersection.

Once the heads at each intersection have been calculated by solving the linear system of equations, the flow can be calculated anywhere in the system by using the relevant analytical expression (which, of course, varies from plane to plane given the particular size and geometry of the intersections of that plane). Reciprocally, if the flows are calculated first, then the heads can be calculated next.

ii) Numerical solution. An alternative is to use a numerical solution for the flow problem in each fracture plane (e.g., see Smith et al., 1985; Andersson and Dverstorp, 1987; Stratford et al., 1990). This will allow the representation of a variable aperture in each fracture plane or of a noncircular geometry of the fractures or even of the partial filling of fractures with permeable sediments or alteration products. A finite element mesh is first generated in each plane. Each intersection is thus discretized with a certain number of nodes; such nodes are common to two intersecting fractures. The linear system of equations is then built by saying that, in steady state, the heads of two intersecting fracture planes are identical at the nodes, and that the algebraic flows calculated along each discretized segment of the intersections are also identical. Of course, the size of the linear system of equations becomes enormous, as there may be hundreds of unknown heads in each fracture plane, depending on the discretization; the final linear system is the sum of all the usual finite element equations in each plane, plus the Kirchhoff relations at the intersections.

There are, however, simplifications that can make the system tractable. One assumes again that the head is constant along each intersection; all nodes on an intersection in the finite element mesh are given the same value. Given that the flow equations are linear, it is then possible to solve the flow problem independently for each fracture plane: one determines numerically, once and for all, the coefficients that, for a given plane, relate the algebraic flow in each intersection of that plane to the constant heads on these same intersections (one can use the principle of superposition to do so). One then writes the same Kirchhoff equations as for the analytical method (i) above. It is also possible to solve numerically for each fracture plane successively even when the heads are kept different along the nodes of an intersection: this only increases the size of the resulting Kirchhoff problem.

An alternative is to use the boundary element method to solve the flow equation in each fracture plane (Andersson and Dverstorp, 1987). Each fracture must, however, have constant properties over its area.

It would be conceivable to extend the numerical approach to transient situations, but this has not yet been done.

iii) Channel model. Cacas (1989) and Cacas et al. (1990a) assumed that in each fracture plane flow did not occur over the whole surface of the fracture, but only in a limited number of "channels." A series of such "channels" are assumed to connect the intersections in a fracture plane to each other. To simplify the problem even further, these authors also assumed (Fig. 4.14.2) that:

a) Each intersection is connected to a fictitious "node" at the center of each circular fracture by a single equivalent straight "channel" starting from the center of the intersection; no assumption is made on the exact geometry of the real channel.

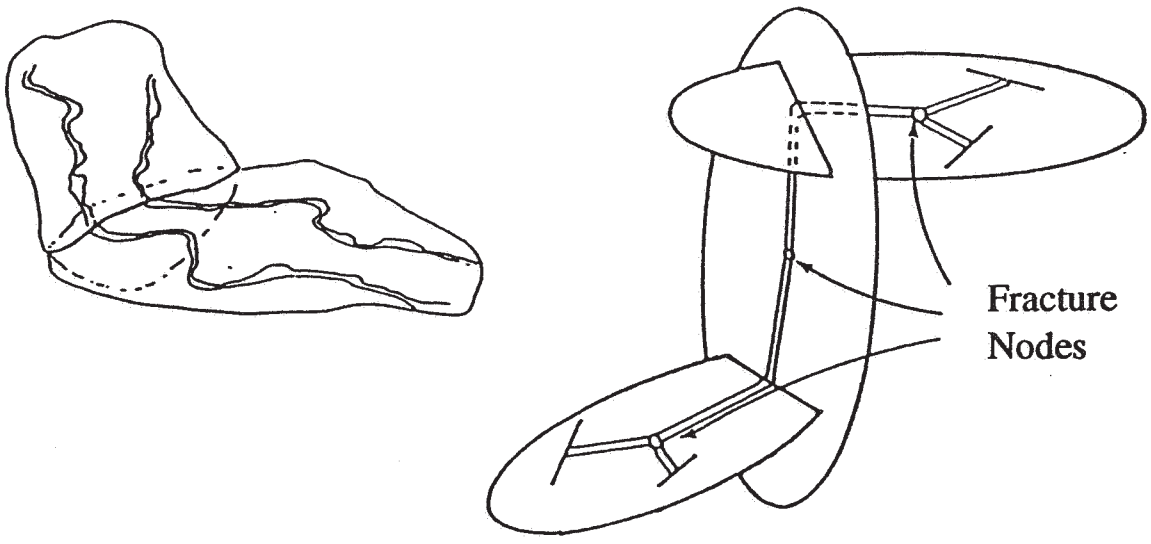

Figure 4.14.2. Channeling in a fracture plane and equivalent "channel model." After Cacas (1989).

b) The property of each equivalent channel is uniquely defined by an equivalent "hydraulic conductivity" K (in cubic meters per second) relating the flow through the channel to the hydraulic gradient within the channel (the difference of heads at the two ends of the channel divided by its length).

c) The head at the fictitious central "node" of each fracture becomes the unknown; note that the number of unknowns is then drastically reduced compared to the previous approach, since there are far fewer fractures than fracture intersections.

d) Between two central nodes of intersecting fractures, two channels are thus in series (one in each fracture plane). The flow through the channels is then given by the harmonic mean of their equivalent "hydraulic conductivity" K_i, weighted by their length:

$$Q = \frac{\Delta H}{L_1 / K_1 + L_2 / K_2}$$

where L_i is the length of each channel and ΔH the head difference between the two central nodes.

e) The equivalent "hydraulic conductivity" K_i for a given fracture plane is assumed identical for all the channels of that plane; K_i can, however, vary from plane to plane.

The mass-balance Kirchhoff relation in steady state is then easily written, with the heads at the central nodes as unknowns, by stating that the algebraic sum of all the flows calculated at each node is zero, again giving as many linear equations as unknowns. This approach could quite easily be extended to transient state, by giving to each central node a "storage coefficient" representing the change in mass in the fracture as a function of the change in head (for compressibility of the water and mechanical opening or closing of the fracture, see, for example, Bruel, 1990 for the mechanical coupling).

In the two previous approaches (i) and (ii), it is conceivable to estimate independently the aperture of the fractures (or its distribution) and to provide that information to the model. On the contrary, the "equivalent hydraulic conductivity" of the channel model cannot easily be anticipated, as it also includes some unknown geometric properties of the channels (e.g., tortuosity and spatial variability), and can thus only be calibrated from local flow experiments. This will be described in section 4.14.2.

One other property of the above channel model is that it might slightly overestimate the connectivity of a network model: as each fracture has a single "equivalent hydraulic conductivity," all the fractures that intersect it will be connected with each other; it could happen, in practice, that only a few fracture intersections within a fracture plane are interconnected, the others being sealed. It might be possible, however, to include such an effect by removing the concerned intersections from the system.

Still, the channel model is numerically the most efficient: it can include the largest number of fractures for a given computational effort (measured in terms of both CPU time and memory).

iv) Multi-channel model. This approach has been suggested, for example, by Billaux (1990). In this case, each fracture plane is said to include a prescribed number of fixed "channels," forming, for example, a network of lines in the plane. Flow can only occur along these lines. They can be generated randomly, as a 2D network of fractures, and they can randomly be given a directional hydraulic conductivity. Tsang and Tsang (1987) used another approach (a random fracture aperture model) to generate the flow channels in the plane.

In each such planar network, the calculation of the flow is again a Kirchhoff problem, the nodes of which are the intersections of the lines, and the unknowns of which are the heads at

these intersections. The intersection between two fracture planes is considered as a particular channel belonging simultaneously to the two intersecting planes, thus forming the link in the global Kirchhoff model with the local Kirchhoff models in each plane. These intersection lines are generally given a larger hydraulic conductivity than the other channels, fracture intersections being in general assumed to be preferential pathways.

This model is very attractive but, again, very demanding in terms of computer resources.

4.14.2 Simplification of the Flow Model

Once a flow model is built, it can be "trimmed" and simplified.

i) First, all fractures that form an isolated cluster not linked to the infinite cluster can be removed, as they do not contribute to the flow (see a definition of the clusters in Sec. 4.13.1). Second, all fractures that have only one connection can also be removed, since no water can flow through them (a minimum of two connections is, of course, required). Different search algorithms are needed to carry out this screening.

ii) Then, another series of fractures may be removed from the model, even if they belong to the infinite cluster. For instance, it can be assumed that, let us say, only 50% of all the fractures are water-conducting; after having generated the network, one can randomly remove 50% of the generated fractures (this could also be done by arbitrarily reducing the density of the fractures during the generation process). A more common practice is to remove fractures according to their aperture or equivalent hydraulic conductivity. Suppose that in the fracture network, each fracture has been given an aperture, or an equivalent hydraulic conductivity, and let us order the fractures by decreasing value of their aperture or hydraulic conductivity (in other words, fracture number 1 has the largest value, and the last fracture the lowest). Let us imagine that the fracture network is now built by locating in space first fracture number 1, then fracture number 2, etc. Until the number of fractures in the domain is large enough for the network to be at the percolation threshold, the fracture medium is globally impervious. However, after the percolation threshold has been reached, adding new fractures with decreasing hydraulic conductivity contributes, after a while, very little to the global permeability of the medium, since the "pervious" fractures have already been located. In practice, one observes that it is not necessary to go very much beyond the percolation threshold, especially if the distribution of the apertures or hydraulic conductivities is large; this would not be true, however, if all fractures had the same properties. One can therefore, in general, reduce the size of the numerical problem by eliminating the less pervious fractures by a procedure opposite to the one just outlined above. Tests must, however, be made to determine how many fractures can be disregarded. One must then repeat step (i).

4.14.3 Stationarity, Ergodicity, Realizations and Averaging

Before going into the calibration of fracture network models, we need to discuss what they actually represent. Let us assume that a "block" of fractured rock (e.g., a cube or a sphere) is to be modeled with a discrete fracture network. As explained in section 4.5, such models are realizations of random sets. Once the statistics of the fracture geometry of the medium to be modeled have been determined, as well as the statistics of the apertures or "equivalent hydraulic conductivities" (as will be explained in section 4.14.4), it is possible to simulate (in the Monte

Carlo sense) an infinite number of equivalent fracture networks. This is done by selecting random numbers and sampling all the properties of a given network from their probability distributions (location, orientation, length, aperture, etc.). If these properties are not independent, correlated sampling must be used (e.g., the length of a fracture and its aperture, if they are correlated).

A single network, with all its fractures located in space and given all their properties, is called a "realization" of the stochastic model. The statistics on which the model is based refer in general to a real rock mass where the observations have been made. What are the relations between a realization and the real medium? They can never be identical, even if conditioning has been used (as described in section 4.9); stochastic models are built precisely because the real medium is unknown (apart from its outcrops), and therefore only the statistics of the description of the medium can be of use when representing what has not been observed.

An underlying assumption is that the statistics of the properties of the medium that have not been observed are identical to those that have. For instance, if a rock mass is analyzed through the examination of the wall of a 100 m-long drift excavated through it, and if the rock block that is to be modeled is a cylinder centered on that drift with a diameter of 100 m and a length of 100 m, the underlying assumption is that the statistics of the fracture properties that have been observed on the wall apply, in fact, to the whole cylinder, which has not actually been observed. This assumption is called "stationarity" and it is the one always used in practice.

One realization of the stochastic model of the rock cylinder will therefore only display one possible arrangement of the fractures in the cylinder; this arrangement, if it were used for determining the statistics of the fracture properties, should, by definition, produce the same statistics as those observed (within the sampling fluctuations, which are a function of the sample size, here the number of fractures in the cylinder). Nothing more can be said about the representativeness of one single realization of the real medium. If the realization has been conditioned on the observations on the drift wall, the fractures on the walls in the model and in the real medium will, by definition, be identical, but this involves such a small part of the rock volume that its global hydraulic behavior is largely unaffected, e.g., as shown by Andersson and Dverstorp (1987). One is therefore faced with the problem that a large number of (equally likely) realizations of the fractured medium need to be considered against a single real rock mass that is to be modeled. This leads us to use averaging.

Let us, however, discuss for a moment the issue of stationarity. One must understand that this is a question of scale. Let us take, for instance, the density of fractures; suppose that we measure the density of fractures along a drift in a mine and find a density d_1 over the first 100 m of the drift; on a later section, a density d_2 different from d_1 is found. Is the medium nonstationary? Yes and no! If our objective is to model a rock block around section 1, we are better off using density d_1 in the stochastic model and assuming that it very well represents the density in the vicinity of section 1; we would similarly use density d_2 in another model in the vicinity of section 2. The medium can be seen as nonstationary but, at a larger scale, if we want to represent a very large rock block including several such sections with different densities, can we simply use an average of the measured local densities? If the variations in the local densities are small enough to be compatible with the normal sampling fluctuations of a pure random model, the medium can be considered, in fact, as globally stationary with a density equal to the average experimental one. If the local densities differ too much, a model with a regionalized density such as the one described in Sec. 4.8.3 can be used; in such a model, the density still remains stationary but displays spatial variations; an application is presented by Long and Billaux

(1987) and Billaux (1990). We would expect from this geostatistical approach a model that is representative of the rock both at the local and global scales, which the pure random model could not do. In some circumstances, such as for modeling an increasing fracture density near the surface, due to decompression, a truly nonstationary model would be needed.

Let us go back to averaging. We cannot compare the real system with one realization, and this is all the more true if there are local property fluctuations that the model neglects because of the stationarity assumption. Can we then compare averages? In the real medium, we can do two kinds of averaging. We can first average over space. We can, for instance, design hydraulic tests that influence a large volume of rock and produce a single average property (e.g. an equivalent continuous medium hydraulic conductivity); this can be done, for example, by long duration pumping tests with distant observation wells. This is the approach used when one is trying to define "representative elementary volumes" in fractured rocks (with the restrictions already discussed in Sec. 4.13.1). We can, however, use other kinds of averaging. We can, for instance, measure locally the property of the medium, e.g., with local injection tests in short sections of boreholes. We can then analyze statistically the distribution of the results of these tests, and, incidentally, not just limit this analysis to the average.

Now what can we do with the stochastic model? We can actually do very similar things. We can design hydraulic tests to be performed numerically on one realization of the model and interpret them in terms of an equivalent hydraulic conductivity. Examples can be found, for instance, in Long (1983) and Long et al. (1982). The hydraulic test was used just to prescribe two different heads on two sides of a cube of rock made of discrete fractures and to measure the flow through the cube in a numerical experiment. If the size of the cube is progressively increased, and if the concept of "representative elementary volume" (REV) applies, one should reach a size beyond which the equivalent hydraulic conductivity no longer fluctuates significantly when the size is varied. This size would be that of the REV of the model. The property determined in this way is a space average of the local model properties obtained from one single realization. This approach has not been very successful so far, because either the concept of REV does not apply to the studied fracture networks or it is impossible, because of computer limitations, to reach the size beyond which the fluctuations are considered small enough to be negligible (a cubic block of 100 m in size may contain millions of fractures that cannot, as yet, be handled by any existing computer). If this approach of averaging could be used, one can anticipate that the same average value would be obtained for any realization of the medium, whereas this is certainly not true for small blocks below the REV size: each realization produces a different average value.

However, we can also perform the other type of averaging on the stochastic model: we can design a small-scale hydraulic test, e.g., with a small cube with two different heads prescribed on two sides, and carry out many such tests on many realizations of the model. As stated before, each realization will give a different equivalent hydraulic conductivity, as the size of the cube is below REV size. Now we can also do the statistics of these tests, among which we can calculate the average.

By doing this, we replace the statistics of the small-scale tests made on the real medium (at different locations in space) with the statistics of the small-scale numerical experiments made on the model (on different realizations). We are allowed to do this if for the fracture network we use an ergodic model, i.e., a model such that all realizations have the same global average density, which is, in practice, the average experimental density. If this average density is not well-known, it is more interesting to study the behavior of the network for some possible values of the density

(especially if the network is near the percolation threshold) rather than to indistinctly mix all the possibilities into a nonergodic model.

The ergodic assumption is thus commonly made, and ensemble statistics of realizations of stochastic fracture network models are indeed compared with spatial statistics of measurements; this is, in fact, one of the ways of calibrating stochastic models, as will be explained in Sec. 4.14.4.

If the ergodic assumption can be used, it is then also possible to determine the large-scale equivalent hydraulic conductivity of the network by making averages of small-scale numerical experiments: the properties at the REV size of the model can be inferred from running many numerical experiments at the small scale, much below that of the REV. It is, however, necessary to assume that the small-scale numerical experiments have carried with them all the major features of the fractured medium properties: at the very large scale, for instance, the role of a major fracture could never be correctly accounted for by the small-scale experiments.

A question arises, however: which type of averaging of the small-scale numerical experiments should be used? Most authors, so far, have intuitively used the arithmetic average, which may be incorrect. If the property of interest is the hydraulic conductivity, it is well known concerning heterogeneous media that averaging hydraulic conductivities is not trivial (e.g., see Matheron 1967). This author has shown, in particular, that the true average always lies between the harmonic and the arithmetic mean. Only in two dimensions, for parallel flow conditions, and if the distribution of the hydraulic conductivity is log-normal and isotropic, is the geometric mean the exact average. If we now consider small block realizations of network models as having "local" properties, and the large-scale equivalent medium as constituted by the small blocks placed side by side, we can use these results and propose that the geometric mean of the realization is probably a better estimate of average model properties, and that harmonic and arithmetic means are the lower and upper brackets, respectively. See, for example, Cacas et al. (1990a).

4.14.4 Calibration of the Flow Model

The issue is here to determine the aperture of the fractures, or the "equivalent hydraulic conductivity" of the channels, in the model. We have indeed seen that these quantities cannot, in general, be determined directly from observation of the fractures on outcrops or cores. It is, however, always possible to assume a priori a value for such parameters (e.g., defined as constant, constant per set of fractures, or random with a given pdf) and to use the stochastic network model in a "what if?" manner: What if the fractured medium happened to have these properties? This can be acceptable for generic studies of fractured media, but it is inadequate for the study of a given real fractured medium.

One would therefore like to infer the hydraulic properties of the fractures from real measurements. So far, injection tests in short sections of boreholes have mostly been used for this purpose, but on one occasion water dripping from the ceiling of a drift in a mine was taken as basic information. Three methods have been proposed.

i) One method is to interpret the injection test as if all the fractures in the tested section are orthogonal to the axis of the borehole, of infinite extension, and have the same aperture; the interpretation of the results of the test can then be given in terms of the equivalent aperture of the fractures with the parallel plate assumption, if the total number of fractures in the section is known (e.g., from the coring or borehole televiewer). Another model is to assume that the

apertures of the fractures of a given section are related to the ones observed on cores; Long and Billaux (1987) assumed, for instance, that the cubes of the real apertures are proportional to observed ones and fit the proportionality coefficient. The shorter the section the better, until, in the end, one single fracture per section is tested. By interpreting several such tests, an idea of the probability distribution function of the apertures can also be obtained. Other methods of interpreting injection tests can also be used, the point being that many tests must be performed and interpreted in order to get a value of the pdf of the aperture, possibly set by set of fractures, as the aperture may be very different according to the orientation if the stress field is very anisotropic.

ii) Another method, proposed by Cacas et al. (1990a), is to use the ergodic assumption outlined in Sec. 4.14.3. A large number of injection tests performed in the real medium are compared with simulated tests on a large number of realizations of the fracture network model; initial assumptions are made on the type of distribution of the apertures (or in this case "equivalent hydraulic conductivity" of channels) and on the parameters of these distributions. By trial and error, the calculated results are compared with the measured ones, the parameters or types of pdf's are changed until the results are considered close enough; the model is then said to be calibrated. In their work, Cacas et al. had 180 injection tests over 2.5-m long sections, and they performed 208 simulations of similar tests on 208 realizations of a spherical fracture network (10 m in diameter) with a central borehole where water was injected at a prescribed head, while the outer surface of the sphere was assumed at constant head. Figure 4.14.3 shows the histograms of the measured and calculated flows in the 2.5-m sections when calibration was obtained. Note that the calibration is not just made on the mean, but on the comparison of the histograms. For their case, they selected a lognormal distribution for the equivalent "hydraulic conductivity" of their channels, which was thus defined by two unknown parameters, a mean and a variance. These two parameters were calibrated by trial and error. They suggested that more parameters could have been calibrated, if, for instance, a different distribution of the hydraulic conductivity of the channels had been selected for each directional set of fractures.

iii) Dverstorp and Andersson (1989) did not use injection tests but observations of the water dripping from the ceiling in a drift in the Stripa mine, collected in 350 plastic sheets glued to the ceiling (see Ch. 2). Assuming the hydraulic gradient to be unity and all fractures reaching a given sheet to have the same aperture, they derived the fracture transmissivity (product of the equivalent hydraulic conductivity by the aperture) and its distribution.

Once the model has been calibrated, i.e., the unknown distributions of the hydraulic conductivities or apertures have been determined, it can be used for simulations. Cacas et al. (1990a) also proposed to validate the model by a change of scale: they used the calibrated model to calculate the large-scale (REV) hydraulic conductivity of the stochastic fracture network, using the averaging method explained in Sec. 4.14.3 and showed that it compared very well with a large-scale hydraulic conductivity determined by a large-scale flow experiment in the real fractured system.

4.14.5 Results Given by Stochastic Fracture Network Flow Models

As presented in section 4.14.3, stochastic fracture network models, once calibrated, can be used to calculate large-scale equivalent hydraulic conductivities of a continuum. They are especially well-suited for determining the anisotropy of this conductivity as exemplified by Long et al.

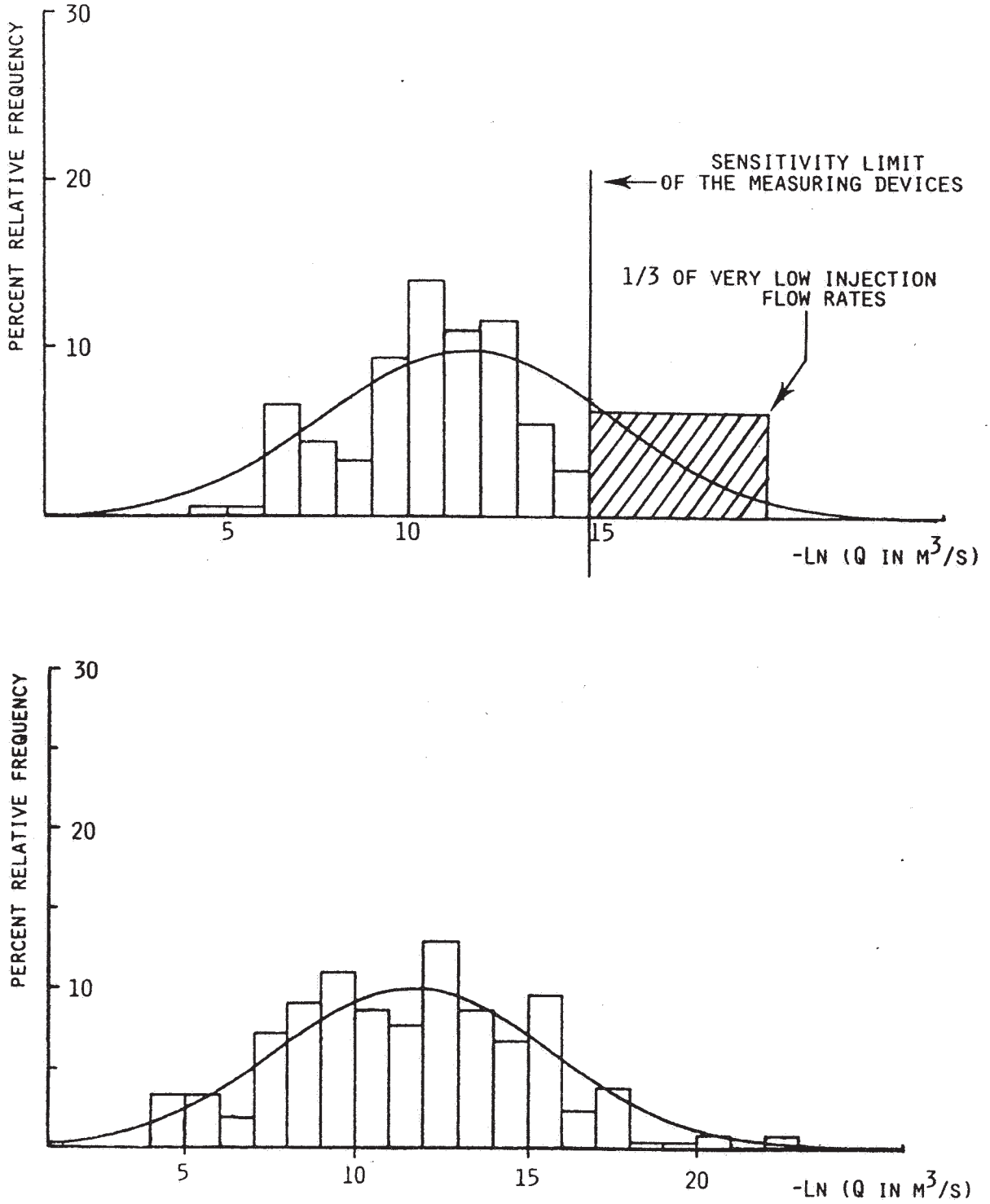

Figure 4.14.3. Histograms of measured and calculated flows in borehole injection tests. After Cacas et al. (1990a).

(1982) and Cacas et al. (1990a). In the numerical flow experiment in a cube, the orientation of the cube can be rotated continuously, by "cutting" the cube for the flow experiment within a larger fixed realization (Fig. 4.14.4); a directional hydraulic conductivity is then calculated along the orientation of the cube. The anisotropy must, however, be determined by averaging the directional hydraulic conductivity of a good number of realizations.

Stochastic fracture network models can also be used directly to solve flow problems but they can only handle problems of a limited size (because of computer limitations, the dimension of a block can only be on the order of tens of meters, if all the water-conducting fractures are to be represented). Examples are the injection of water into deep hot dry rock wells for hydraulic fracturing (Bruel, 1990), and calculation of the variability of the flux of water coming into a deposition hole in a granitic nuclear waste repository (Dverstorp, 1990). In the latter case the interest of the stochastic model is to show, with many realizations, the distribution of the flow rates in the deposition holes and not just the mean: the corrosion rates of the canisters is indeed a function of this flow rate, and for safety studies the distribution is sometimes more important than the mean.

It would also be possible to predict fracture flow around the walls of a dam; this would similarly show the uncertainty of the predictions if a large number of realizations of the fracture network were run with the same boundary conditions and, possibly, conditioned by the same set of observations on the walls of the valley. A coupled mechanical-hydraulic model (Bruel, 1990) should be used to take into account the potential build-up of underpressures below the dam and its potential consequences for the dam stability.

It would be possible to represent a larger flow domain (e.g., in kilometers) only if the number of fractures introduced into the model were drastically reduced. This could be done, for example, by keeping only the largest fractures; it is not clear, however, if the largest fractures alone will create a percolating network or if some of the smaller fractures must be introduced in order to raise it above the percolation threshold. This topic deserves further research.

4.15 USE OF STOCHASTIC FRACTURE NETWORK MODELS FOR TRANSPORT PROBLEMS

Most of what has been explained in general for flow models can be extended to transport models. We will therefore only present the specifics of discrete fracture transport models.

4.15.1 Building the Transport Model

The method most widely used to represent transport in a stochastic fracture network model is the "particle following" method (Robinson, 1984; Cacas et al., 1990b; and Nordqvist et al., 1992). It is, of course, first necessary to build a flow model; the transport is then calculated for each realization of the model. We describe below the method as applied to a channel model (or along lines in 2D).

In its original form, the particle following method consists in following discrete particles added to the flow, whose trajectories are determined from the flow pattern. The main assumptions are the following: (i) the particles are moved by advection only (longitudinal dispersion is disregarded); (ii) chemical reactions and sorption are not taken into account; and (iii) diffusion both in the fluid and in the rock matrix is neglected.

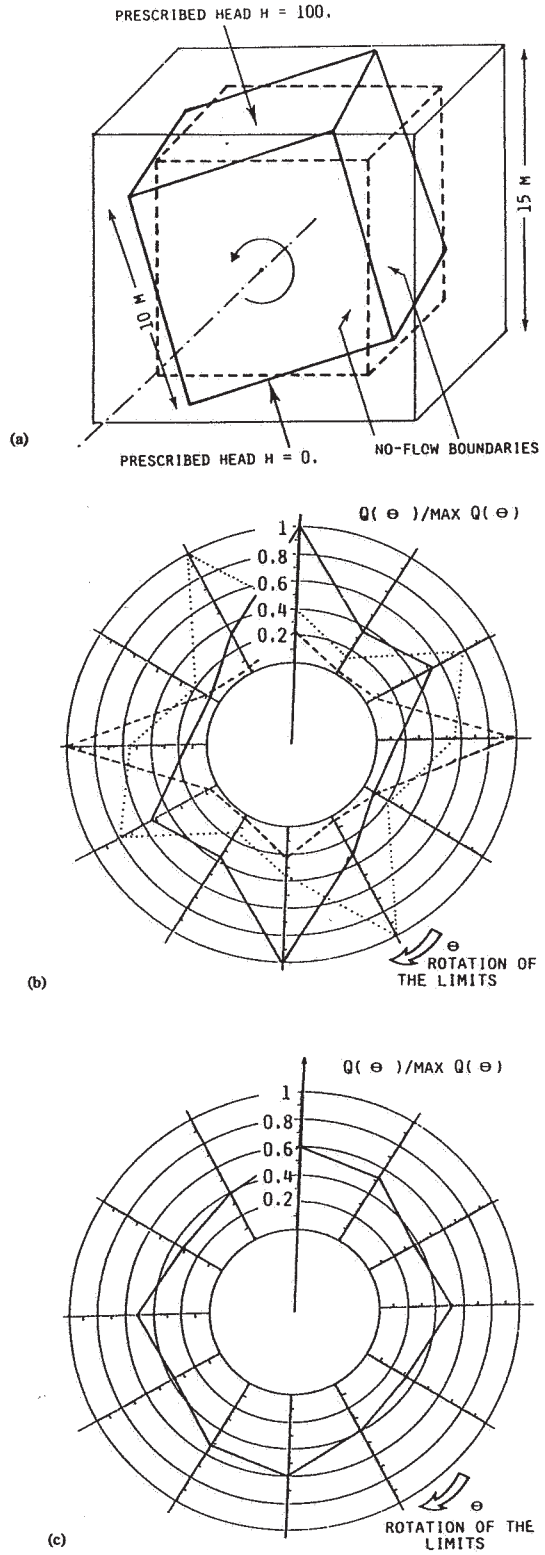

Figure 4.14.4. Determination of the anisotropy of a fracture model, after Cacas et al. (1990a): a) selection of the orientation of a fracture network cube in a realization for a numerical experiment; b) directional hydraulic conductivity of three realizations; c) average directional hydraulic conductivity of 17 realizations.

The particle trajectories are drawn at random according to the following rules: (i) The particle trajectory is divided into elementary steps corresponding to the displacement between two adjacent connections. An average travel time is computed at each step. It is inferred from the flow rate and the volume of the channel through which the particle travels. The total residence time of a particle along its path is given by the summation of the elementary travel times computed at each step from the entrance to the exit points. (ii) When the particle arrives at a new connection, the next channel through which it is going to move is drawn at random. The assumption of a perfect mixing of the different fluxes entering a connection is made (Fig. 4.15.1a). Therefore the probability that the particle will follow a given channel is proportional to the ratio of its flow rate to the total flux that goes through the connection.

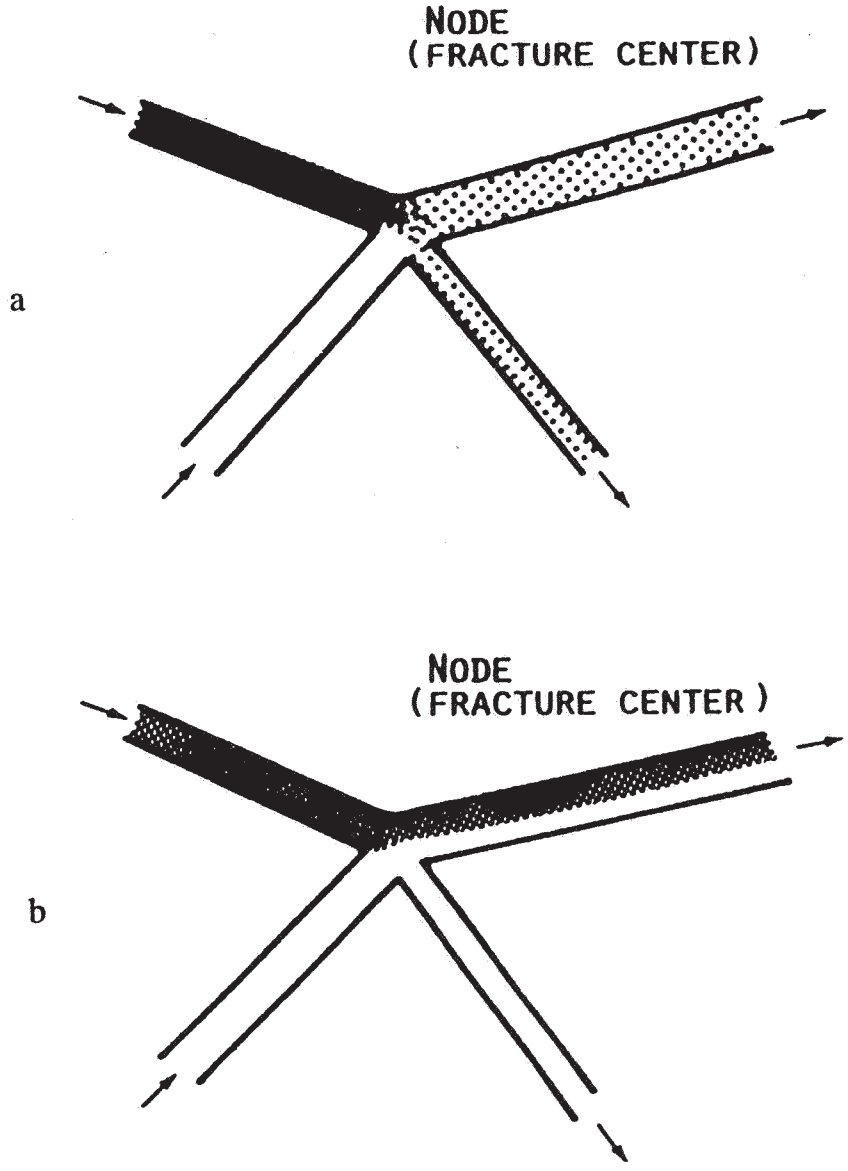

Figure 4.15.1. Mixing assumptions at fracture intersections, after Cacas et al. (1990b): a) perfect mixing; b) no mixing.

The assumption of complete mixing at each fracture node needs to be discussed (e.g., see Novakowski et al., 1985, and Philip, 1988). In practice, perfect mixing at the nodes means that all the outflows of a given fracture of the model have the same tracer concentration. In the assumption of laminar flow, the streamlines define stream tubes with a constant flow rate (Endo et al., 1984), as shown in Fig. 4.15.1b. In the case of a dense and well-connected network of channels inside the fracture surface, the complete mixing hypothesis tends to be realistic because of the spreading of the stream tubes over all the different paths open to the flow, thus creating an intense microscopic dispersion. Conversely, if the channel network is sparse and not connected, the tracer moves in a few preferred paths and no mixing occurs.

The particle-following method could easily take into account biased mixing or even no mixing in the fractures; but no field experiments have yet been carried out that have yielded quantitative results concerning the tracer mixing in channelized fracture flow.

In the channel model, since the exact geometry of the channels is not known, the volume of the channel used to calculate the travel time when the flow rate is known is a parameter of the model; Cacas et al. (1990b) calculated this volume by first assuming that each channel was a straight cylindrical pipe; the radius of this pipe was calculated assuming that the hydraulic resistance of the channel, as calibrated in the flow model, was that of laminar flow in a smooth cylinder: this gives the smallest possible volume of each channel. They then had to multiply this volume by a constant number, identical for all channels, to obtain calibration with tracer test data, without changing the hydraulic resistance of the channels. This multiplying factor was one of the two parameters of the transport model. After the fitting, this number turned out to be on the order of 32 for a fractured granite (see Sec. 4.15.2). This can easily be explained since a "channel" in a fracture plane is far from being a straight cylindrical pipe: its hydraulic diameter varies along the path, and the sections with a small diameter control the hydraulic conductivity, whereas the sections with a large diameter control the total volume of the channel. The hydraulic calibration can estimate the hydraulic diameter of the small sections, but only information obtained through tracer tests can provide the means necessary for the calibration of the diameter of the large sections. The calibrated value of 32 for the multiplying factor thus shows that the channels have an equivalent mean diameter approximately 6 times larger than their hydraulic conductivity would imply. The second parameter of the model is an extension of the original particle-following method to include, approximately, some longitudinal microscopic hydrodynamic dispersion. This is done by randomly modifying the average residence time at each step. The velocity in each channel is perturbed by the addition of a random number normally distributed with zero mean and standard deviation sigma given by:

$$\sigma = \frac{1}{T_m}\sqrt{2U\alpha T_m}$$

where T_m is the average residence time (in s), α is the microdispersivity coefficient in the fracture plane (in m), and U is the average velocity in the channel (in m/s). The dispersion created in this way is an approximation of the 1-D Fickian model of dispersion. α is thus the second parameter of the transport model.

To represent transport, several tens of thousands of particles are injected successively into the model at the entrance (a point, a line, or a surface) and their exit points and transit times are calculated. A histogram of this transit time at any exit point can then be calculated and represents the breakthrough curve for a slug injection of tracer at the entrance point. Other injection patterns

can be calculated by convolution. No concentration within the domain can be calculated, however.

This model is computationally very efficient.

When the flow model is made of finite element meshes for each fracture plane, it is possible to solve the usual convection-dispersion equation in each fracture with mass transfer from fracture to fracture at the intersections. This becomes computationally very demanding but would provide an in situ concentration. Stratford et al. (1990) improved this approach by calculating response functions for each fracture plane for a step tracer injection and then assembling these response functions in series along the flow path by convolution.

4.15.2 Calibration of the Transport Model

In any fracture network transport model, a number of parameters must be calibrated from comparison with tracer experiments. These parameters essentially represent porosity and microscopic dispersion, as, for example, in the Cacas et al. (1990b) model, where only two parameters were defined, representing average properties for the whole model. These parameters must be derived from a comparison of the model outputs with experiments. However, there is one difficulty that frequently crops up here: generally only a few tracer tests are available and furthermore, they more often than not represent transport over different distances of the fractured medium. For a given transport distance, one therefore has just one experiment to compare with the model results and, by definition, a stochastic fracture network model will provide as many results as realizations.

This contrasts with the calibration of a flow model, where in general many injection tests with the same geometry can be compared with a large number of realizations of the stochastic medium. Cacas et al. (1990b) proposed a way out of this dilemma. In their case, four tracer tests were available, on four independent pathways with different lengths; they assumed that all four tests were characterizing the same fractured medium on which a stochastic flow model had already been calibrated; thus they had two parameters to calibrate on these four tests. They developed four different submodels, each representing one of the four tracer tests, with its particular geometry, distance, flow conditions, etc. They then characterized each test by a few global numbers, e.g., time of arrival of the peak concentration, the total breakthrough duration (for a slug injection of tracer), or the time of first arrival. Several realizations of each tracer test were then made, from which a histogram of the corresponding numbers for each test could be established (they used only time of peak arrival and total breakthrough duration).

For a single test, it is impossible to compare one such number with a histogram: there are no valid reasons why the experimental value should fall around the mean of the histogram, nor why it should be on the right or on the left of the distribution. However, when four tests are compared simultaneously, it is justified to require that all four tests should not simultaneously be on the same side of their histograms: if this were the case, one could logically assume that the model was biased.

It thus becomes possible to calibrate the model by modifying its parameters until the four tests are reasonably well distributed over their respective histograms. This is shown in Fig. 4.15.2 a,b. The four calculated histograms of the time of peak arrival (a) or (open circles) breakthrough duration (b) are shown, one for each tracer test; a star also shows the single measured value for the corresponding test; it is easy to see that the model is approximately calibrated, since for test

a

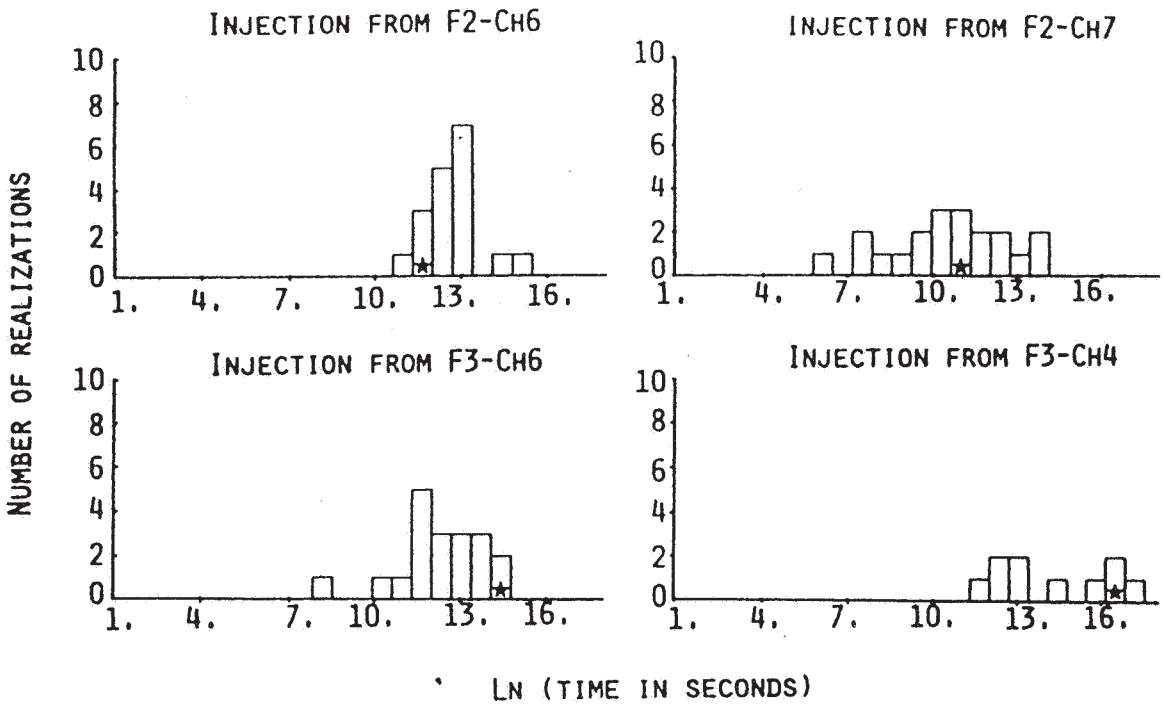

b

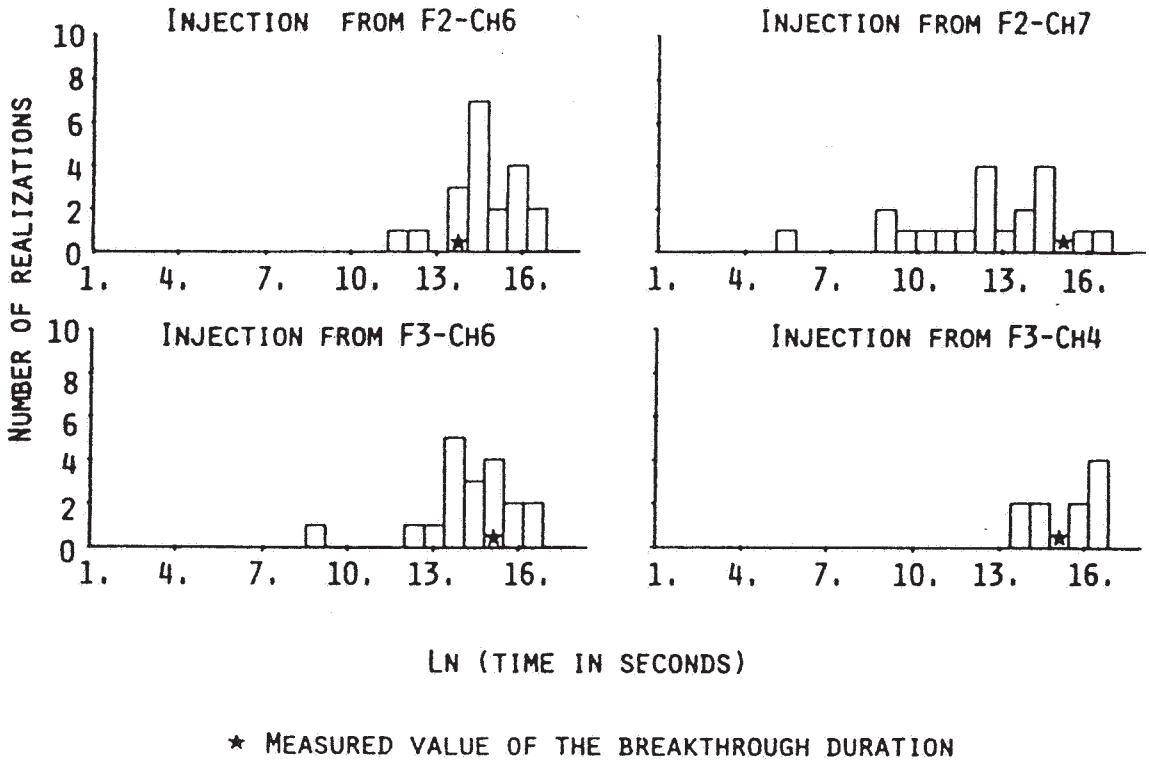

Figure 4.15.2. Calibration of a stochastic transport model, after Cacas et al. (1990b): a) comparison of observed and calculated peak arrival times; b) comparison of observed and calculated breakthrough durations.

F2-CH6 the star is on the left side of the histogram, for F2-CH7, it is on the right side, for F3-CH6, on the right side, and for F3-CH4, it is close to the middle, in Fig. 4.15.2a, and the same argument also applies to Fig. 4.15.2b. It was with this comparison that the first multiplying parameter of 32 quoted in Sec. 4.15.1 was obtained.

The second parameter of the Cacas et al. (1990b) model, representing longitudinal microscopic dispersion, was calibrated by comparing the "smoothness" of the calculated responses with the actual breakthrough curves measured in the field; Fig. 4.15.3 is a sensitivity study of the response of the model to the α parameter of the longitudinal microscopic dispersion, as explained in section 4.15.1. From this sensitivity study, a value of α of 0.8 m was selected. Note that this microscopic longitudinal dispersion introduced in the particle-following algorithm only provides a small part of the global dispersion; most of the global longitudinal dispersion and all of the transverse dispersion is given by the connections between the different channels in the fracture network. No additional parameter can modify the transverse dispersion, at least in the Cacas et al. (1990b) model, which is only due to the branching-out of the different fractures in the geometric network. Tracer tests are thus a way to validate the geometry of the fracture network model, by comparing observed and calculated transverse dispersion.

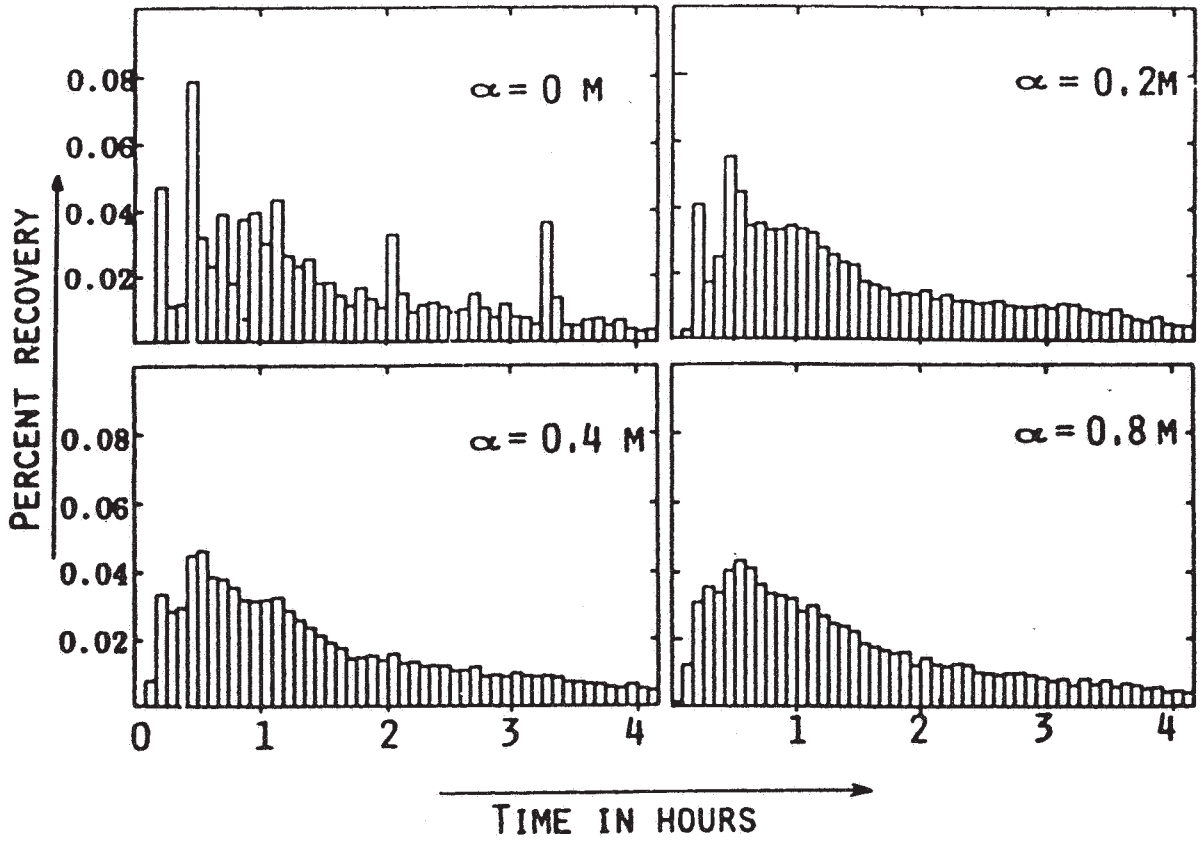

Figure 4.15.3. Study of the sensitivity of the channel transport model to the microdispersion parameter α. After Cacas et al. (1990b).

To actually determine the real transverse dispersion of the fracture system from the observations it is necessary to observe the "spread" of the tracer in a direction orthogonal to the main flow direction; in a two-well tracer test, this is impossible; it can, however, be done in an underground test, when a tracer is injected into a borehole and recovered at the walls of a drift, as in Cacas et al. (1990b) or Nordqvist (1992). In such a case, the observed "spread" of the tracer in the drift is compared, for each tracer test, with the calculated spread for an ensemble of realizations.

4.15.3 Representation of Matrix Diffusion

To represent matrix diffusion in a discrete fracture network model (or to represent sorption or chemical reactions), a method of representing transport other than the particle-following algorithm must be used. When the flow model is made of finite element meshes for each fracture plane and the usual convection-dispersion equation is solved in each fracture, then matrix diffusion (or sorption and chemical reactions) can be introduced as in any numerical model. For the channel model, concentrations must be calculated at each node of the model by first solving an advection equation in each channel of the model and then a mass balance equation at each node. Perfect mixing of all the fluxes coming from each channel connected to a node is assumed. Matrix diffusion (or sorption and chemical reactions) can be included in this mass balance equation assuming that at each node a given area of the fracture is available for contact with the fluid. Preliminary tests of this method can be found in Cacas (1989) or Bruel (1990) for a thermal problem, where heat conduction in the unfractured rock takes the place of matrix diffusion.

4.15.4 Results Given by a Stochastic Fracture Network Transport Model

Like the flow models, the discrete fracture network transport models are severely limited by the size at which they can represent transport. Thus their use is presently limited to the interpretation of tracer tests or to the prediction of transport over small distances, e.g., tens or hundreds of meters at most. Their advantage over more classical continuous models is that they can help to predict the probability of existence of a "short-circuit" in a given rock mass made of connected fractures. When the flow and transport properties of the discrete model have been calibrated, one can indeed run transport calculations over a large number of realizations on the distance of interest and determine the percentage of the results that show "rapid" transit, defined as a given fraction of the mean travel time. This percentage can then be seen as the probability that, in the real medium, a "short-circuit" may exist over the given travel path. Any other statistics of the travel time can be determined just as well.

4.16 OTHER STOCHASTIC FRACTURE MODELS

Neuman (1988) has suggested another method of stochastically representing a fractured medium. It is based on continuous equivalent medium representation on a regular grid (finite differences or finite elements); each grid block being given an equivalent hydraulic conductivity value.

The generation of several possible such hydraulic conductivity fields is made in three steps: (i) a large number of injection tests performed in the medium over small injection chambers are interpreted using one of the usual analytical expressions describing such tests, e.g., the Dupuit or

Lugeon formulas; (ii) the variogram of these local values is determined with a geostatistical analysis; and (iii) conditional simulations of the hydraulic conductivity are generated using the procedure described, for example, by Delhomme (1979).

As in discrete fracture network models, the method needs a large number of realizations of the fractured medium in order to analyze its behavior, not just a single one; the author also claims that the size of the grid blocks on which the conditional simulations are done can be on a smaller scale than the representative elementary volume of the fracture network, since the domain investigated by the injection tests can also be below the size of the REV. The geostatistical simulations are a means to generate the below-REV spatial variability of the medium.

One of the problems of this approach is, however, that it assumes that the analytical expressions used to interpret the injection tests provide representative local values, which may not always be true. Cacas (1989) has tried to determine to what extent such local radial tests are representative of the true local hydraulic conductivity of the medium. Using a theoretical 3D discrete fracture network model representing a cube, she simulated radial injection tests in such cubes and determined numerically, for 155 realizations, the local hydraulic conductivity K using the classical formula

$$K = \frac{Q}{L\Delta H}$$

(Louis, 1974), where Q is the calculated injection flow rate, L is the length of the injection chamber, and ΔH is the prescribed increase in hydraulic head in the chamber. This formula assumes that the radius of influence R of an injection test is

$$R = r_0 e^{2\pi}$$

where r_0 is the radius of the injection chamber.

She then determined the local hydraulic conductivity of the same theoretical fractured medium by running parallel flow experiments in a cube on the same realizations, as explained in Sec. 4.14.5 and Fig. 4.14.4. She observed that, whatever the variance of the hydraulic conductivity of the channels, the distribution of the hydraulic conductivity given by the radial tests had a larger variance than that of the parallel flow experiment in a cube, and furthermore, that the mean of the former was about 5 times larger than that of the latter.

These results should be taken with some caution since they apply to a theoretical model and not to a real medium. They show, however, that using classical analytical expressions to interpret injection tests in fractured media may not always be justified. Using discrete fracture network models to make such interpretations, as explained in Sec. 4.14.4, may be a better approach.

4.17 CONCLUSION

Stochastic methods can realistically model and simulate the geometry of actual fracture fields. Much care must be taken during the statistical study of the fractures because of the numerous bias sources that affect the data. Network models of variable sophistication are available. The parameters of the 3D models can be deduced from 1D and 2D surveying. Simulations visualize the possible 3D geometry of reality and can be conditioned to the actual data.

Several approaches can be used to study the variability at the scale of the single fracture. The reduction of fracture networks to channel networks opens new ways, such as the comparison with media of noninteger dimension or the analogy with regular lattice networks.

There is obviously a need for further development. In the field of geometric modeling, it would be useful to develop models that take into account the chronology of the brittle deformation that generated the fractures as well as the mechanism of crack propagation (e.g., Granier, 1985; Meakin, 1990). This may involve refinements in the survey and modeling techniques, for example in order to describe the points where some fractures are stopped by others (Gervais et al., 1992). Concerning the shape of the single fracture and its effect on flow, the above-mentioned approaches have to be investigated in more depth. This should lead to new developments concerning the general hydraulic behavior of fractured fields and its link with connectivity.

Concerning flow and transport modeling, the assumptions of channeling in the fracture plane for various rock types and history should be further investigated; the degree of mixing at channel or fracture intersections should also be experimentally examined. More efficient computer codes capable of handling a larger number of fractures and thus of representing a larger rock volume should be developed. The linking of discrete fracture network models with more usual continuous models should also be considered in order to have local discrete representations of fractured media imbedded in discretized continuous models.

REFERENCES

Andersson, J., and Dverstorp, B. Conditional simulations of fluid flow in three-dimensional networks of discrete fractures, *Water Resour. Res.*, vol. 23(10), p. 1876–1886, 1987.

Andersson, J., Shapiro, A.M., and Bear, J. A stochastic model of fractured rock conditioned by measured information, *Water Resour. Res.*, vol. 20(1), p. 79–88, 1984.

Baecher, G.B, and Lanney, N.A. Trace length biases in joint surveys, *Proceedings,* 19th US Symp. Rock Mechanics, AIME, vol. 1, p. 56–65, 1978.

Baecher, G.B., Lanney, N.A., Einstein, H.H. Statistical description of rock properties and sampling, *Proceedings,* 18th US Symp. Rock Mechanics, AIME, p. 5C1:1–8, 1977.

Bailey, A.I. A method of analyzing polymodal distributions in orientation data, *Math. Geol.*, vol. 7(4), p. 285–293, 1975.

Barker, J. A generalized radial flow model for hydraulic tests in fractured rock, *Water Resour. Res.*, vol. 24(10), p. 1796–1804, 1988.

Barla, G., Scavia, C., Antonellis, M., and Guarascio, M. Characterization of rock mass by geostatistical analysis at the Masua mine, *Proceedings,* 6th Int. Congr. Rock Mechanics, ISRM, Montreal, vol. 2, p. 777–786, 1987.

Barton, C.C. Fractal analysis of the scaling and spatial clustering of fractures in rock. In: "Fractals and their application to geology," *Proceedings*, 1988 GSA Annual Meeting Symposium on Fractals, GSA, in press, 1992.

Barton, C.C., and Larsen, E. Fractal geometry of two-dimensional fracture networks at Yucca Mountain, southwestern Nevada, *Proceedings*, Int. Symp. on Fundamentals of Rock Joints, Bjorkliden, p. 77–84, 1985.

Billaux, D. Influence de la connectivité d'un réseau de fractures sur sa réponse à un essai de pompage, *Rock at Great Depth-Rock Mechanics and Rock Physics at Great Depth*, Proceedings of an International Symposium, Pau, 28-31.08.89, V. Maury and D. Fourmaintraux (eds.), 1620 p., 3 vols., Hfl.295, A.A. Balkema, P.O. Box 1675, Rotterdam, p. 473–480, 1989.

Billaux, D. Hydrogéologie des milieux fracturés. Géométrie, connectivité et comportement hydraulique, Ph.D. thesis, Ecole des Mines, Paris, 277 p., 1990.

Billaux, D., Chilès, J.P., Hestir, K., and Long, J. Three-dimensional statistical modeling of a fracture rock mass – an example from the Fanay-Augères mine, *Int. J. Rock Mech. Min. Sci. and Geomech. Abstr.*, vol. 26(3/4), p. 281–299, 1989.

Broadbent, S.R., and Hammersley, J.M. Proc. Camb. Phil. Soc., Vol. 53, p. 629, 1957.

Brown, S.R., and Scholz, C.H. Broad bandwidth study of the topography of natural rock surfaces, *J. Geophys. Res.*, vol. 90(12), p. 575–582, 1985.

Bruel, D. Exploitation de la chaleur des roches chaudes et sèches. Etude des phénomènes hydrauliques, mécaniques et thermiques au moyen d'un modèle à fractures discrètes, Ph.D. thesis, Ecole des Mines de Paris, Fontainebleau, 161 p., 1990.

Cacas, M.C., Ledoux, E., de Marsily, G., Tillie, B., Barbreau, A., Durand, E., Feuga, B., and Peaudecerf, P. Modeling fracture flow with a stochastic discrete fracture network: 1. The flow model, *Water Resour. Res.*, vol. 26(3), p. 479–489, 1990a.

Cacas, M.C., Ledoux, E., de Marsily, G., Barbreau, A., Calmels, P., Gaillard, B., and Margritta, R. Modeling fracture flow with a stochastic discrete fracture network: 2. The transport model, *Water Resour. Res.*, vol. 26(3), p. 491–500, 1990b.

Cacas, M.C. Développement d'un modèle tridimensionnel stochastique discret pour la simulation de l'écoulement et des transports de masse et de chaleur en milieu fracturé, Ph.D. thesis, Ecole des Mines de Paris, Fontainebleau, 1989.

Charlaix, E., Guyon, E., and Rivier, N. A criterion for percolation threshold in a random array of plates, *Solid State Communication*, vol. 20(11), p. 999–1002, 1984.

Chelidze, T.L. Percolation and fracture, *Physics of Earth and Planetary Interiors*, vol. 28, p. 93–101, 1982.

Chilès, J.P. Fractal and geostatistical methods for modeling a fracture network, *Math. Geol.*, vol. 20(6), p. 631–654, 1988.

Chilès, J.P. Three-dimensional geometric modelling of a fracture network, *Geostatistical Sensitivity, and Uncertainty Methods for Ground-Water Flow and Radionuclide Transport Modeling*, B.E. Buxton (ed.), Battelle Press, Columbus, Ohio, p. 361-385, 1989a.

Chilès, J.P. Modélisation géostatistique de réseaux de fractures, *Geostatistics*, M. Armstrong (ed.), Kluwer Academic Publ., Dordrecht, Netherlands, Vol. 1, p. 57–76, 1989b.

Chilès, J.P., and Gentier, S. Geostatistical modeling of a single fracture. *Proceedings*, 4th Int. Geostatistics Congress, Troia, Portugal, 1992, to be published.

Chilès, J.P., Guérin, F., and Billaux, D. 3D stochastic simulation of fracture network and flow at Stripa conditioned on observed fractures and calibrated on measured flow rates, *Rock Mechanics*, J.R. Tillerson and W.R. Wawersik (eds.), Balkema, Rotterdam, Netherlands, p. 533-542, 1992.

Clerc, J.P., Giraud, G., Roussenq, J., Blanc, R., Carton, J.P., Guyon, E., Ottavi, H., and Stauffer, D. La percolation: modèles, simulations analogiques et numériques, *Annales de Physique*, vol. 8(1), p. 5–105, 1983.

Conrad, F., and Jacquin, C. Représentation d'un réseau bidimensionnel de fractures par un modèle probabiliste. Application au calcul des grandeurs géométriques des blocs matriciels, *J. of IFP*, vol. 28(6), p. 843–890, 1973.

Courrioux, G., and Jacquot, T. Etude de l'effet de coupe dans l'interprétation des diagrammes de pétrofabrique: application au granite de Beauvoir (Echassières, Massif Central Français). *Comptes Rendus*, Académie des Sciences, Paris, vol. 299, série II(9), p. 549–554, 1984.

Cruden, D.M. Describing the size of discontinuities, *Int. Rock. Mech. Min. Sci. and Geomech. Abstr.*, vol. 14, p. 133–137, 1977.

de Marsily, G. Flow and transport in fractured rocks. Connectivity and scale effect. In: Hydrogeology of Rocks of Low Permeability, *Memoires Int. Assoc. Hydrogeol.*, vol. 17, p. 267–277, 1985.

de Marsily, G. *Quantitative Hydrogeology, Groundwater Hydrology for Engineers*, Academic Press, New York, 440 p., 1986.

Delhomme, J.P. Kriging in the hydrosciences, *Advances in Water Resources*, vol. 1(5), p. 251–266, 1978.

Delhomme, J.P. Spatial variability and uncertainty in groundwater flow parameters: a geostatistical approach, *Water Resour. Res.*, vol. 15(2), p. 269–280, 1979.

Dershowitz, W.S. Rock joint systems, Ph.D. thesis, MIT, Cambridge, Mass., 764 p., 1984.

Dershowitz, W.S., and Einstein, H.H. Characterizing rock joint geometry with joint system models, *Rock Mechanics and Rock Engineering*, vol. 21, p. 21–51, 1988.

Dienes, J.K., 1982 Permeability, percolation and statistical crack mechanism. Issues in Rock Mechanics, Proc. 22nd Symp. on Rock Mechanics, Berkeley, Univ. of Calif. Aug. 1987.

Diggle, P.J., and Fisher, N.I. Sphere: a contouring program for spherical data, *Computer and Geosciences*, vol. 11(6), p. 725–766, 1985.

Dverstorp, B., and Andersson, J. Application of discrete fracture network concept with field data: possibilities of model calibration and validation, *Water Resour. Res.*, vol. 25(3), p. 540–550, 1989.

Dverstorp, B. Report to SKI, Royal Institute of Technology, Stockholm, 1990.

Dverstorp B., and Andersson, J. Estimation of effective transport parameters for predictive use in fractured rock, (1991), *Water Resour. Res.*, to appear,

Endo, H.K., Long, J.C.S., Wilson, C.R., and Witherspoon, P.A. A model for investigating mechanical transport in fracture networks, *Water Resour. Res.*, vol. 20(10), p. 1390–1400, 1984.

Engelman, R., Gur, Y., and Jaeger, Z. Fluid flow through a crack network in rocks, *J. Applied Mechanics*, vol. 50, p. 707–711, 1983.

Feder, J. *Fractals*, Plenum Publ. Corp., New York, 283 p., 1988.

Feuga, B. Hydrogeologic modeling of fractured rock, *Jornadas sobre modelos matematicos aplicables al almacenamiento de residuos radioactivos*, Esc. Sup. de Engenieros de Minas, Madrid., 1986.

Gentier, S. Morphologie et comportement hydromécanique d'une fracture naturelle dans un granite sous contrainte normale, Ph.D. thesis, Univ. of Orléans, Doc. BRGM no. 134, 597 p., 1986.

Gentier, S., Chilès, J.P., and Riss, J. Analyse et simulation d'une surface de fracture rocheuse. *Cahiers de Géostatistique*, Fasc. 1, ENS des Mines de Paris, p. 77–87, 1991.

Gervais, F., Chilès, J.P., and Gentier, S. Geostatistical analysis and hierarchical modeling of fracture network in a stratified rock mass, *Proceedings, Fractured and Jointed Rock Masses*, Lake Tahoe, California, to be published by A.A. Balkema, Rotterdam, 1992.

Granier, T. Origin, damping and pattern of development of faults in granite, *Tectonics*, vol. 4(7), p. 721–737, 1985.

Grossman, N.F. The bivariate normal distribution on the tangent plane at the mean attitude, *Proceedings,* Int. Symp. on Fundamentals of Rock Joints, Bjorkliden, Sweden, p. 3–11, 1985.

Guyon, E., Hulin, J.P., and Lenormand, R. Applications de la percolation à la physique des milieux poreux, *Les Annales des Mines*, vol. 5-6, p. 17–40, 1984.

Hestir, K., and Long, J. Analytical expression for the permeability of random two-dimensional Poisson fracture networks based on regular lattice percolation and equivalent media theories, J. Geoph. Res., vol. 95, B13, p. 21565–21581, 1990.

Jacquin, C.G., and Adler, P.M. Fractal porous media. II. Geometry of porous geological structures, *Transport in Porous Media*, 2, p. 571–596, 1987.

Kendall, M.G., and Moran, P.A. *Geometrical probability.* Hafner, New York, 1963.

Kirkpatrick, S. Percolation and conduction. *Rev. of Modern Physics*, vol. 45(4), p. 574–588, 1975.

La Pointe, P.R. Analysis of spatial variation in rock mass properties through geostatistics, *Proceedings,* 21st US Symp. on Rock Mechanics, Rolla, Missouri, p. 570–580, 1980.

Laslett, G.M. Censoring and edge effect in areal and line transect sampling of rock joint traces, *Math. Geol.*, vol. 14(2), p. 125–140, 1982.

Lewis, T., and Fisher, N.I. Graphical methods for investigating the fit of a Fisher distribution to spherical data, *Geophys. J.R. Astr. Soc. 69*, p. 1–13, 1982.

Loiseau, P., 1987. Etude structurale et géostatistique des gneiss de la région du Cézallier: modélisation tridimensionnelle de réseaux de fractures; application à l'écoulement des fluides, Ph.D. thesis, University of Orléans, Doc. BRGM no 162, 1988, 200 p.

Long, J.C.S. Investigation of equivalent porous media permeability in networks of discontinuous fractures, Ph.D. thesis, Lawrence Berkeley Laboratory, Univ. of California, Berkeley, CA, 1983.

Long, J.C.S. Modeling of fluid flow and transport in fracture networks, *Jornadas sobre modelos matematicos aplicables al almacenamiento de residuos radioactivos*, Esc. Sup. de Engenieros de Minas, Madrid, 1986.

Long, J.C.S., Remner, J.S., Wilson, C.R., and Witherspoon, P.A. Porous media equivalents for networks of discontinuous fractures, *Water Resour. Res.*, vol. 18(3), p. 645–658, 1982.

Long, J.C.S., and Billaux, D. From field data to fracture network modeling: An example incorporating spatial structure, *Water Resour. Res.*, vol. 23(7), p. 1201–1216, 1987.

Louis, C. Introduction à l'hydraulique des roches, *Bull. Bur. Rech. Géol. Min.*, Ser. 2, Sec. III, vol. 4, 1974.

Mancktelow, N.S. A least-square method for determining the best-fit point maximum, great circle and small circle to nondirectional orientation data, *Math. Geol.*, vol. 13(6), p. 507–521, 1981.

Mandelbrot, B.B. *The Fractal Geometry of Nature*, Freeman, New York, 468 p., 1983.

Mandelbrot, B.B. Self-affine fractals and fractal dimension, *Physica Scripta*, vol. 32, p. 257–260, 1985.

Mandelbrot, B.B., Passoja, D.E., and Paullay, A.J. Fractal character of fracture surfaces of metals, *Nature*, vol. 308, p. 721–722 , 1984.

Mantoglou, A. Digital simulation of multivariate two- and three-dimensional stochastic processes with a spectral turning bands method, *Math. Geol.* vol. 19(2), p. 129–149, 1987.

Mardia, K.V. *Statistics of Directional Data.* Academic Press, London, 357 p., 1972.

Massoud, H., 1987. Modélisation de la petite fracturation par les techniques de la géostatistique, Ph.D. thesis, Ecole des Mines, Paris, Doc. BRGM no. 155, 1988, 210 p.

Matérn, B. Spatial variation. Stochastic models and their application to some problems in forest surveys and other sampling investigations, *Meddelande fran Statens Skogsforskningsinstitut*, vol. 49(5), Almaenna Foerlaget, Stockholm, 144 p., 1960.

Matheron, G. *Les variables régionalisées et leur estimation. Une application de la théorie des fonctions aléatoires aux Sciences de la Nature*, Masson, Paris, 306 p., 1965.

Matheron, G. *Eléments pour une théorie des milieux poreux*, Masson, Paris, 1967.

Matheron, G. Les polyèdres poissoniens isotropes, *Actes du 3e Colloque Européen sur la fragmentation*, Cannes, II-9, p. 509–534, 1971.

Matheron, G. *Random Sets and Integral Geometry*, Wiley, New York, 1975.

Meakin, P. Simple models for crack growth. In: Crystal Properties and Preparation on "Elastic and Plastic Properties of Crystals," Trans. Tech Publications, Aedermannsdorf, Switzerland, 1990.

Miles, R.E. Poisson planes in Euclidean space. Part I: A finite number of random uniform flats. *Advances in Applied Probability*, no 1, p. 211–237, 1969.

Miles, R.E. The random division of space. *Special Supplement to Advances in Applied Probability*, p. 243–266, 1972.

Miller, S.M. Geostatistical analysis for evaluating spatial dependence of fracture set characteristics. *Proceedings,* 16th A PCOM Symp., SME-AIME, New York, p. 537–545, 1979.

Neuman, S.P. A proposed conceptual framework and methodology for investigating flow and transport in Swedish crystalline rocks, a position paper submitted to SKB. Ref. SKB 88-37, Stockholm, Sweden, 1988.

Nordqvist, A.W., Tsang, Y.W., Tsang, C.F., Dverstorp, B., Andersson, J. A variable aperture fracture network model for flow and transport in fractured rocks, *Water Resour. Res.*, vol. 28(6), p. 1703–1713, 1992.

Novakowski, K.S., Gordon, V.E., David, A.L., and Kenneth, G.R. A field example of measuring hydrodynamic dispersion in a single fracture, *Water Resour. Res.*, vol. 21(8) p. 1165–1174, 1985.

O'Sullivan, F. A statistical perspective on ill-posed inverse problems, *Stat. Sci.*, vol. 1(4), p. 502–527, 1986.

Pahl, P.J. Estimating the mean length of discontinuity traces, *Int. J. Rock Mech., Min. Sci. and Geomech. Abstr.* vol. 18, p. 221–228, 1981.

Philip, J.R. The fluid mechanics of fractures and other junctions, *Water Resour. Res.*, vol. 24(2) p. 239 – , 1988.

Priest, S.D., and Hudson, J.A. Discontinuity spacings in rock, *Int. J. Rock Mech., Min. Sci. and Geomech. Abstr.*, vol. 13, p. 135–148, 1976.

Robinson, P.C. Connectivity of fracture systems. A percolation theory approach, Ph.D. thesis, St. Catherine's College, Oxford Univ., UK, 1984.

Rouleau, A. Statistical characterization and numerical simulation of a fracture system. Application to a groundwater flow in the Stripa granite, Ph.D. thesis, Univ. of Waterloo, Ontario, Canada, 1984.

Santalo, L.A. *Integral Geometry and Geometric Probability*, Addison-Wesley, Reading, Mass., 434 p., 1976.

Schaeben, H. A new cluster algorithm for orientation data, *Math. Geol.*, vol. 16(2), p. 139–153, 1984.

Serra, J. *Image Analysis and Mathematical Morphology*. Academic Press, London, 628 p., 1982.

Shante, V.K.S., and Kirkpatrick, S. An introduction to percolation theory, *Adv. Phys.*, vol. 20, p. 325–357, 1971.

Smith, L., Maze, C.W., and Schwartz, F.W. A stochastic model for transport in networks of planar fractures, *Int. Symp. on the Stochastic Approach to Subsurface Flow*, Int. Ass. of Hydraulic Res., Montvillargenne, France, G. de Marsily, ed., 1985.

Snow, D.T. A parallel plate model of fractured permeable media, Ph.D. thesis, Univ. of California, Berkeley, 331 p., 1965.

Snow, D.T. The frequency and apertures of fractures in rock, *Int. J. Rock Mech. Min. Sci.*, vol. 7, p. 23–40, 1970.

Stoyan, D., Kendall, W.S., and Mecke, J. *Stochastic Geometry and Its Applications*, Wiley, New York, 1987.

Stratford, R.G., Herbert, A., Jackson, C.P. A parameter study of the influence of aperture variation on fracture flow, and consequences on fracture network, Proc. ISRM Rock Joint Conference, Balkema, Amsterdam, 1990.

Terzaghi, R.D. Sources of error in joint surveys, *Geotechnique*, vol. 15(3), p. 287–303, 1965.

Thomas, A. Structure fractale de l'architecture de champs de fractures en milieu rocheux. *Comptes Rendus*, Acad. Sci., Paris, vol . 304, ser. II(4), p. 181–186, 1987.

Tsang, Y.W., and Tsang, C.F. Channel model of flow through fractured media, *Water Resour. Res.*, vol. 23(3), p. 467–479, 1987.

Veneziano, D. Probabilistic model of joints in rock, unpub. manuscr., MIT, Cambridge, Mass., 1978.

Vere-Jones, D. Statistical theories of crack propagation, *Math. Geol.*, vol. 9, 445, 1977.

Warburton, P.M. A stereological interpretation of joint tracer data, *Int. Rock Mech. Min. Sci. and Geomech. Abstr.* vol. 17, p. 181–190, 1980.

Wilke, S., Guyon, E., and de Marsily, G. Water penetration through fractured rocks : test of a tridimensional percolation description, *Math. Geol.*, vol. 17(1), p. 17–27, 1985.

Yow, J.L. Jr. Blind zones in the acquisition of discontinuity orientation data, *Int. J. Rock Mech. Min. Sci. and Geomech. Abstr.*, vol. 24(5), p. 317–318, 1987.